Pulmonary BCG induces lung resident macrophage activation and confers long-term protection against tuberculosis

Elena Mata[1,2,3] Raquel Tarancon[1,2,4], Claudia Guerrero[1,2], Eduardo Moreo[1,2], Flavie Moreau[5], Santiago Uranga[1,2], Ana Belen Gomez[1,2], Dessislava Marinova[1,2], Miriam Domenech[2,6], Fernando González-Camacho[2,6], Marta Monzon[7], Juan Badiola[7], Jorge Dominguez-Andrés[8], José Yuste[2,6], Alberto Anel[9], Antonio Peixoto[5], Carlos Martin[1,2,10,+], Nacho Aguilo[1,2,*,+]

[1] Grupo de Genética de Micobacterias, IIS Aragón. Universidad de Zaragoza, Facultad de Medicina. C/ Domingo Miral s/n, 50009 Zaragoza, Spain.

[2] CIBER Enfermedades Respiratorias, Instituto de Salud Carlos III, Madrid, Spain.

[3] Current affiliation: Certest Biotec, San Mateo de Gállego, 50840, Zaragoza, (Spain)

[4] Current affiliation: Meakins-Christie Laboratories, Department of Medicine, McGill University Health Centre, McGill University, Montreal, QC, Canada.

[5] Institut de Pharmacologie et de Biologie Structurale (IPBS), Université de Toulouse, CNRS, UPS, Toulouse, France

[6] Centro Nacional de Microbiología. Instituto de Salud Carlos III, Madrid, Spain

[7] Research Centre for Encephalopathies and Transmissible Emerging Diseases, Universidad de Zaragoza, Zaragoza, Spain.

[8] Department of Internal Medicine and Radboud Center for Infectious Diseases (RCI), Radboud University Nijmegen Medical Center, Nijmegen, The Netherlands.

[9] Grupo Apoptosis, Inmunidad y Cáncer, IIS Aragón. Dpto. Bioquímica y Biología Molecular y Celular, Fac. Ciencias, Universidad de Zaragoza, Zaragoza, Spain.

[10] Servicio de Microbiología, Hospital Universitario Miguel Servet, ISS Aragón, Paseo Isabel la Católica 1-3, 50009 Zaragoza, Spain.

* Correspondence: naguilo@unizar.es

[+]Shared senior authorship

One Sentence Summary: Pulmonary BCG administration induces protection against tuberculosis infection via lung macrophage activation.

ABSTRACT

Bacille Calmette-Guerin (BCG) is an attenuated bacterial vaccine used to protect against *Mycobacterium tuberculosis* (*Mtb*) in regions where infections are highly prevalent. BCG is currently delivered by the intradermal route, but alternative routes of administration are of great interest, including intrapulmonary delivery to more closely mimic respiratory *Mycobacterium tuberculosis* (*Mtb*) infection. In this study, mice subjected to pulmonary delivery of GFP-tagged strains of virulent (*Mtb*) and attenuated (BCG) mycobacteria were studied to better characterize infected lung cell subsets. Profound differences in dissemination patterns were detected between *Mtb* and BCG, with a strong tendency of *Mtb* to disseminate from alveolar macrophages (AMs) to other myeloid subsets, mainly neutrophils and recruited macrophages. BCG mostly remained in AMs, which promoted their activation. These pre-activated macrophages were highly efficient in containing *Mtb* bacilli upon challenge and disrupting early bacterial dissemination, which suggests a potential mechanism of protection associated with pulmonary BCG vaccination. Respiratory BCG also protected mice against a lethal *Streptococcus pneumoniae* challenge, suggesting that BCG-induced innate activation could confer heterologous protection against respiratory pathogens different from *Mtb*. Importantly, BCG drove long-term activation of AMs, even after vaccine clearance, and these AMs reacted efficiently upon subsequent challenge. These results suggest the generation of a trained innate memory-like response in AMs induced by pulmonary BCG vaccination.

INTRODUCTION

The BCG vaccine has been in use for nearly a century, but tuberculosis (TB) remains a leading cause mortality caused by a single pathogen and was responsible for ~1.4 million deaths worldwide in 2019 *(1)*. Moreover, the rising threat of multi- and extremely-drug resistant strains makes TB an urgent global health problem and highlights the need for a more effective TB vaccine approach.

There is a renewed interest in strategies based on the delivery of BCG by non-canonical administration routes and intravenous (i.v.) BCG vaccination has recently been shown to induce protection in non-human primates (NHP). Vaccination with BCG by the pulmonary route was first described in clinical studies conducted several decades ago (*2, 3*), and results in multiple preclinical models demonstrated substantial improvements in protection conferred by pulmonary vaccination relative to subcutaneous or intradermal immunization (*4, 5*). Most of the studies describing mucosal immune responses elicited specifically by pulmonary BCG have been focused on adaptive responses. Th17 cells as well as TB-specific mucosal immunoglobulins have been reported to be induced following pulmonary BCG immunization both in mice (*6*) and non-human primates (*7*). However, little is known about the contribution of local innate immunity to vaccine-induced protection.

Mycobacterium tuberculosis (*Mtb*) entry into the airways results in interactions of bacilli with lung phagocytic cells results, and these interactions dictate infection outcomes that can range from sterilization to bacterial dissemination. Mycobacteria are engulfed by alveolar macrophages (AMs) located in the airways during the initial stages of infection, and infected cells rapidly migrate to the lung interstitium where bacilli can disseminate to other phagocytic cells, mainly interstitial macrophages (IMs) differentiated and neutrophils (*8*). These cell populations present differential tolerability

to *Mtb* replication. Interstitial macrophages are highly inflammatory and efficiently impair bacterial replication (*9, 10*), although some macrophage subsets appear to be more permissible to infection (*11*). Neutrophils are typically more permissive to infection and have been associated with bacterial dissemination during active TB (*12-14*).

In the present study, we characterized the activation of lung macrophages induced by pulmonary BCG vaccination, and the contribution of these macrophages to protection against TB. Our results suggest a key role of cell-to-cell spread by *Mtb* during early infection, and how disruption of this dissemination process may be adapted into a protective vaccination approach.

RESULTS

Differential early cellular dissemination pattern between Mtb and BCG

We first characterized infected lung cell populations at different timepoints of pulmonary infection following an intranasal (i.n.) challenge with the virulent *Mtb* strain H37Rv expressing the green fluorescent protein (GFP) (Fig. S1). A low-dose i.n. *Mtb* challenge represents one of the most physiological relevant models of TB infection in mice, but a low bacterial burden makes it difficult to discriminate infected cells from the baseline fluorescence of uninfected cells (*15*). For this reason, we performed challenge experiments with a high dose of 10^6 CFU H37Rv to evaluate infected populations at day 1 and 7 post-infection. At days 13 and 24, we used 10^5 and 10^4 CFU, respectively, to limit disease-associated symptoms and premature mortality at these later timepoints (Fig. 1A). As expected, alveolar macrophages (AMs) ($CD11c^{high}CD64^{+}SiglecF^{+}$) were found to be the main infected subset at early timepoints following i.n. challenge. However, at later timepoints a larger fraction of infected cell had a phenotype consistent with neutrophils ($CD11c^{-}CD64^{-}SiglecF^{-}CD11b^{+}Ly6G^{+}$) (Fig. 1B, C, S2A), and this result correlated with increased neutrophilia in the lungs throughout the infection course (Fig. S2B). Further analysis indicated that interstitial macrophages (IMs) ($CD11c^{dim}CD64^{+}SiglecF^{-}$) were recruited to the lung from day 13 post-infection (Fig. S2B), and that *Mtb* spreads from AMs to IMs during the course of infection, (Fig. 1B, D and Fig. S2A), which confirms previously published observations (*8*).

We next examined whether early *Mtb* dissemination was associated with virulence or served as a strategy to combat infection. We evaluated bacterial dissemination patterns of a GFP-expressing BCG vaccine because this is an attenuated strain that can be controlled by the host immune system upon respiratory infection (*16*). We analysed infected cell populations following i.n. administration of BCG, at the same timepoints

studied for H37Rv (Fig. 1E). RD1 (Region of Difference 1) deficiency in BCG represents the main cause of attenuation and impaired infective capacity (*17*), so we included a BCG strain complemented with RD1 (BCG::RD1), which has been previously reported to restore virulence (*16*). The same dose of 10^6 CFU was used for both BCG and BCG::RD1 (Fig.1E), as no additional toxicity was detected with BCG::RD1 at later timepoints. Although an increase of uninfected neutrophils was observed at day 24 in the lungs of BCG infected mice (Fig. S2B), the vaccine strain barely spread into neutrophils and remained associated with macrophages at all time points measured (Fig. 1F and Fig. S2A), unlike the observed dissemination of H37Rv. A subset of neutrophils infected with BCG::RD1 was detected at day 13 post-infection (Fig. 1G), and this correlated with the restored virulent phenotype of the complemented BCG strain defined by a higher proportion of total BCG::RD1-infected cells and a greater bacterial burden in the lungs of infected mice relative to the BCG group (Fig.S3). At day 13 and 24, BCG::RD1 transitioned into IMs (Fig. 1I), similar to that observed with *Mtb* (Fig. 1D). This bacterial dissemination pattern was not observed with BCG, which was primarily restricted to AMs and had limited spread to IMs by day 24 (Fig.1H and Fig.S2A).

In order to confirm the *Mtb* spread *in situ*, we used confocal microscopy to visualize *Mtb* and BCG acquisition by lung cells at day 1 and 13 post-infection. We infected a transgenic mouse line obtained from the cross of Csf1r-eCFP (Macblue) (*18*) and LysM-GFP mice (*19*) with either H37RV-RFP (red-fluorescent protein) or BCG-RFP. In this mouse line, monocytes and macrophages are CFP (cyan-fluorescent protein) positive whereas mature neutrophils are GFP positive but CFP negative, and this allows for visualization of bacteria by neutrophils in infected lungs. Our results showed that a higher number of neutrophils (GFP^{pos} CFP^{neg}) were recruited to the infected lung after H37Rv infection compared with BCG. (Fig. 1J) In line with our flow cytometry data, neutrophils

(GFP^{pos} CFP^{neg}) acquired H37Rv as early as 24 hours (3%) after infection, with a higher percentage (20%) observed at day 13 after infection (Fig. 1K). In contrast, BCG was rarely if at all detected in neutrophils (GFP^{pos} CFP^{neg}).

We conducted a challenge experiment with H37Rv following neutrophil depletion to better define the role of neutrophils during early infection. Neutrophil depletion was carried out using a combination of the anti-Ly6G (clone 1A8) mAb with a secondary mouse anti-rat-IgGκ (Fig. S4A) (*20*). To assess cell depletion, neutrophils were detected as CD11c^{-}CD11b^{+}Ly6c^{dim} cells (Fig. S4B), as the neutralizing antibody reportedly used in this protocol masks the binding of the anti-Ly6G antibody employed for flow cytometry detection (*20*). We obtained an average reduction of around 65% of neutrophils in lungs measured at day 19 post-infection (Fig. S4B), and we observed a strong decrease of *Mtb*-infected neutrophils relative to non-depleted mice (a reduction from 60% to 20% of the infected cells) at this time point. Under these conditions of reduced neutrophilia, we found that bacteria were not retained within AMs regardless of neutrophil removal, and they mostly migrated to IMs (Fig. S4C). Unexpectedly, lower neutrophil infection levels did not correlate with differences in bacterial burden or the proportion of infected cells, which did not dramatically differ between depleted and non-depleted groups (Fig. S4D, E). This observation suggests that neutrophil colonization might not be a crucial determinant for *Mtb* replication *in vivo*, and bacterial infection might progress successfully in other cellular compartments such as IMs. Interestingly, we found that both infected and total IMs showed lower expression of the activation marker MHCII in the depleted group (Fig. S4F). This observation suggested that neutrophils may contribute to optimal activation of bystander IMs, which may explain the permissibility of these cells to allow *Mtb* replication under these conditions.

Pulmonary but not subcutaneous BCG vaccination induces lung macrophage activation

We next studied the expression of well-known activation markers in BCG-infected macrophages. We observed a time-dependent increase of MHCII, CD86 and iNOS in the BCG-containing cells (GFP^+) (Fig. 2A). Interestingly, pulmonary BCG also triggered the activation of bystander uninfected macrophages (GFP^-) (Fig. 2B), which is consistent with previous studies (*21*). A similar trend was observed when macrophages were infected with GFP-expressing H37Rv (Fig. S5), albeit with more rapid kinetics, suggesting that macrophage activation occurs independently of bacterial virulence levels.

We evaluated macrophage activation induced by i.n. or subcutaneous (s.c.) vaccination by immunizing mice with 10^6 CFU of BCG and analyzing macrophage activation at four or eight weeks post-vaccination (Fig. 2C). BCG bacteria were detected in the lungs at both timepoints following i.n. immunization, but no detectable BCG colonies were found in mice that received s.c. BCG (Fig. 2D). I.n. BCG, but not s.c. BCG, induced macrophage activation at four and eight weeks post-vaccination (Fig. 2E), suggesting that the physical presence of BCG may be required to trigger macrophage activation, but this comparison could not be made here as s.c. BCG did not result in lung colonization.

We analyzed differences in the gene expression profiles of AMs at eight weeks post-i.n. BCG vaccination. Selected target genes were followed based on their roles in inflammation and metabolism, including glycolysis, because expression of these genes has been associated with long-term innate cell activation (*22*). We observed the sustained upregulation of several genes associated with an inflammatory profile of macrophages, including *Nos2*, *Ifng*, *Irf8* or *Ccl2* (Fig. 2F). Of note, several of the most upregulated genes are related to increased metabolic function in these cells, such as *Hk2*, *Ldlr*, *G6pdx*

or *Ldha*. The upregulation of these pathways has been described as a hallmark of the induction of trained immunity both at a central level and in alveolar macrophages (*23*, *24*).

BCG-activated macrophages contain early infection and prevent *Mtb* spread from AMs

These observations led us to hypothesize that i.n. BCG-pre-activated AMs could represent a primary containment barrier against a subsequent *Mtb* infection. To test this hypothesis, we immunized mice with a non-fluorescent BCG (10^6 CFU) by the i.n. or s.c. route and challenged mice 8 weeks later by i.n. delivery of a GFP-expressing H37Rv strain (Fig. 3A). We compared activation markers of *Mtb*-infected cells in naïve versus vaccinated mice. Our data revealed that AMs infected with *Mtb* (GFP^+) at day one post-challenge are already present at an activated status in the i.n. BCG group and are positive for the three inflammatory markers analyzed (MHCII, CD86 and iNOS) (Fig. 3B). In contrast, the activation status of *Mtb*-infected AMs from mice immunized with s.c. BCG was lower and similar to unvaccinated controls.

Importantly, analysis of infected (GFP^+) cells revealed restricted (low) dissemination of *Mtb* into neutrophils in lungs of i.n. vaccinated mice (Fig. 3C, S6A), and virulent mycobacteria were typically localized to the macrophage compartment at both time points (Fig. 3D). I.n BCG was associated with fewer uninfected neutrophils in the lungs relative to unvaccinated controls (Fig. S6B). These observations correlated with a strong vaccine-induced protective effect, demonstrated by a reduced bacterial burden in lungs (Fig. 3E) in the i.n. BCG group compared with unvaccinated controls. S.c. BCG vaccination resulted in a similar dissemination profile to the unvaccinated controls, with a higher proportion of infected neutrophils compared to the i.n. BCG group. There was a

substantial decrease of infected neutrophils by day 24 (Fig. 3C, S6A), which correlated with control of infection (Fig. 3E).

Analysis of macrophage subsets indicated that *Mtb* was mainly restricted to AMs in the i.n. BCG-vaccinated mice, suggesting that previously activated AMs dramatically limited the capacity of *Mtb* to spread to other cellular compartments (Fig. 3F, S6A). Both unvaccinated and s.c.-vaccinated mice showed a progressive bacterial spread from AMs to IMs throughout the infection. A higher proportion of infected IMs was detected at day 7 post-challenge in the s.c. vaccinated group compared with unvaccinated mice (Fig. 3F), which is consistent with previous studies and may be a potential mechanism of protection induced by s.c. BCG (*25*).

We evaluated the compartmentalization of the lung myeloid cells that were infected *in vivo*. Anti-CD45 antibody was administered i.v. route prior to sacrifice to discern immune cells recruited from circulation versus cells resident in the lung tissue (Fig. S7A). As expected, no $CD45^+$ AMs were found in the lungs of either vaccinated or unvaccinated mice, indicating that this cellular population is lung tissue-resident (Fig. S7B). In contrast, we found a large proportion of $CD45^+$ neutrophils (around 50%), with no differences observed between the different groups, which indicated a constant influx of neutrophils from the circulation to the lungs. Similarly, the presence of $CD45^+$ IMs reflected recruitment of these cells from the blood to the lung parenchyma, although the proportion of circulating cells was found to be higher early after challenge, decreasing progressively throughout the infection (Fig. S7B). Of note, no GFP+ cells were found in $CD45^+$-circulating cells, indicating that infection occurs once cells extravasate from circulation into the lung tissues (Fig. S7C, D).

We analyzed the proliferation marker Ki67 in infected and uninfected lung macrophages following challenge. Interestingly, a dramatically higher proportion of

Ki67-expressing infected (GFP+) AMs was observed in the i.n. BCG group compared with the s.c. BCG group and unvaccinated controls at day 1 post-challenge. This higher Ki67 expression was maintained at all the analyzed time points and was restricted to infected cells. This result suggests that i.n. BCG-primed AMs proliferate upon *Mtb* infection, which could represent a mechanism contributing to early protection associated with i.n. BCG vaccination (Fig. S8).

Macrophages can recognize a broad range of pathogens. Therefore, we hypothesized that BCG-activated lung macrophages may protect against a respiratory bacterial infection different from TB. Eight weeks after i.n. or s.c. BCG vaccination, mice were challenged i.n. with a lethal dose of *Streptococcus pneumoniae* and animal survival was assessed (Fig. 3H). Five out of 10 mice from the i.n. vaccinated group did not show any disease-associated symptoms at the end of the experiment (7 days post-challenge), whereas all the animals from the unvaccinated group reached endpoint criteria and were sacrificed (Fig. 3H). A slight, but not significant protection was found in the s.c.-vaccinated group, with 2 out of 10 survivors at the end of the study. Intranasally-vaccinated mice also showed a lower degree of disseminated bacteria in blood at 24, 48- and 72-hours post-challenge compared with unvaccinated controls and to the s.c. vaccinated group (Fig.3I).

CD4$^+$ T cells contribute to vaccine-induced macrophage activation

IFN-γ production by CD8$^+$ T cells has been described as a key cytokine for the priming and activation of AMs in response to respiratory viral infection (*24*). We have previously reported that i.n. BCG induces a strong local antigen-specific T cell response (*4, 6*). In the present work, we aimed to assess the importance of T cells in BCG-induced macrophage activation and early protection against *Mtb*.

We evaluated vaccine-induced antigen specific T cell responses at different timepoints pre- and post-challenge by analyzing IFN-γ-producing lung $CD4^+$ and $CD8^+$ cells in vaccinated and unvaccinated mice. $CD4^+$ T cell-specific IFN-γ induction was substantially higher than $CD8^+$ T cells, confirming that mycobacteria preferentially trigger $CD4^+$ T cell-dependant responses. Our data revealed that i.n. BCG induced IFN-γ-producing $CD4^+$ cells at all the timepoints tested, including at day 1 before challenge (Fig. S9A-C). Conversely, s.c. BCG-induced lung responses were delayed until day 7 post-challenge. In addition, we measured IFN-γ protein concentration in lung suspensions from i.n. BCG -vaccinated mice following $CD4^+$ or $CD8^+$ T-cell depletion, which it was highly effective for both populations (>95%) (Fig. S10). IFN-γ levels were profoundly reduced in the absence of $CD4^+$ cells and not CD8+, which suggested that $CD4^+$ T lymphocytes were major producers of this cytokine following pulmonary BCG vaccination (Fig. S9D, E).

Based on these results, we assessed the role of $CD4^+$ T cells for lung macrophage activation. Mice were vaccinated with i.n. BCG, and $CD4^+$ T cells were depleted at the time of *Mtb* infection, Antibody-mediated depletion of $CD4^+$ T cells was initiated one week prior to challenge (Fig. 4A), which allowed for these cells to be present during the vaccination phase. Our results revealed that *Mtb*-infected AMs (GFP^+ cells) analyzed one day after i.n. challenge remained activated in the absence of $CD4^+$ T cells, confirmed by expression of MHCII and CD86 (Fig. 4B). We found lower expression of iNOS in the $CD4^+$ T cell-depleted group, suggesting that specific activation markers in AMs might be triggered by interactions with $CD4^+$ T cells. Bacterial dissemination into neutrophils at day 13 (Fig. 4C), as well as lung *Mtb* bacillary load were lower in the i.n. BCG-vaccinated $CD4^+$ T cell-depleted group (Fig. 4E) compared with unvaccinated controls, suggesting that BCG-activated macrophages induced protection even in the absence of

283 $CD4^+$ T cells. We conducted a survival experiment using a low-dose i.n. *Mtb* challenge
284 and treated mice with anti-CD4 antibodies weekly for the duration of the challenge phase,
285 with depletion starting prior to *Mtb* inoculation. We observed reduced survival in $CD4^+$
286 T cell-depleted unvaccinated mice, whereas survival was not affected in the BCG-
287 immunized animals, regardless of the presence of $CD4^+$ T cells (Fig. 4F). These results
288 suggest that early protection conferred by BCG-activated innate cells may be effective
289 for longer periods of time.

290 We assessed the effect of $CD4^+$ T cell depletion during vaccination and challenge
291 phases (Fig. 4G). The absence of $CD4^+$ T cells during vaccination led to deficient
292 activation of AMs, which internalized *Mtb* upon challenge and had lower expression of
293 MHCII, CD86 and iNOS markers (Fig. 4H). Analysis of infected cell populations at day
294 13 post-challenge indicated lower retention of *Mtb* in macrophages from the $CD4^+$ T cell-
295 depleted group in comparison to vaccinated control mice (Fig. 4I), and higher
296 dissemination into neutrophils (Fig. 4J) at levels similar to unvaccinated controls. In
297 addition, *Mtb* burden at day 13 was comparable in the $CD4^+$ T cell-depleted group and
298 unvaccinated mice (Fig. 4K), suggesting the need for $CD4^+$ T cell-mediated activation of
299 macrophages for vaccine-induced protection.

300 We assessed the contribution of $CD8^+$ T cells to BCG-induced macrophage
301 activation (Fig. S11). The absence of $CD8^+$ T cells during vaccination and/or challenge
302 phases had no significant effect on AM activation and bacterial burden in lungs.

303 **Pulmonary BCG induces long-term activation of AMs**

304 We examined the effects of long-term macrophage activation following BCG
305 vaccine clearance, as this is critical to identifying the acquisition of a memory-like
306 phenotype by innate cell populations (*26*). We hypothesized that the enhanced responses
307 upon a secondary *Mtb* challenge may be due to memory acquisition and not due to the

presence of the primary stimuli. We vaccinated mice with i.n. BCG and evaluated bacterial clearance at different time points after immunization (Fig. 5A). Some BCG bacteria were found in the lungs at five months, but not at seven months (Fig. 5B). We also characterized different myeloid populations with the objective of evaluating cellular infiltration events accompanying bacterial clearance (Fig. 5C). Our data revealed a strong correlation between the amount of pulmonary BCG and the level of infiltrated IMs (Fig. 5C, D). The number of neutrophils was elevated in the vaccinated group at one month post-vaccination (Fig. 5D). IM and neutrophil infiltration disappeared by seven months (fixed end-point of experiment), suggesting that the vaccine-induced inflammatory state was resolved upon bacterial clearance, and the lung immunological environment returned to homeostasis.

AMs detected at seven months post-vaccination showed high expression of MHCII and CD86, indicating that these cells maintained some degree of activation after vaccine clearance in comparison to age-matched unvaccinated controls (Fig. 5E). iNOS expression was not significantly different between vaccinated and naïve groups, which differed from observations in the short-term vaccination experiments. We assessed expression of the genes studied in two month-vaccination experiments (Fig. 2F) in sorted AMs from month seven. In this case, only *Ldlr*, *Irf8* and *Il1b* expression levels were dramatically upregulated in sorted AMs, such that basal expression of inflammatory markers detected two months after vaccination had nearly disappeared by month seven (Fig S12).

Certain subsets of innate cells have been shown to undergo a shift toward a memory-like phenotype, which is characterized by increased responsiveness to secondary stimulation (*24, 27, 28*). Mice were challenged with GFP-expressing H37Rv as secondary stimulus seven months after i.n. BCG vaccination (Fig. 5F), and the expression level of

activation markers were measured on infected (GFP^+) and uninfected (GFP^-) AMs at day one post-challenge. We assumed that GFP-negative cells in both vaccinated and unvaccinated groups were not likely to trigger a secondary response as they had not interacted directly with challenge bacteria. Our data demonstrated that AMs from i.n. BCG group behaved as that predicted for a memory-like response, with a substantial increase in activation marker expression in infected cells relative to uninfected cells (Fig. 5G). This was particularly notable for iNOS, because long-term activated AMs had reduced expression of this marker (Fig. 5E) that increased rapidly upon secondary stimulation.

Importantly, as we had shown for short-term vaccination experiments, bacterial dissemination of neutrophils at day 13 post-challenge was dramatically reduced under these conditions (Fig. 5H), with mycobacteria mostly contained within macrophages (Fig. 5I). Bacillary loads (CFU) in the lungs of vaccinated mice were also lower as compared to unvaccinated controls (Fig. 5J), suggesting that BCG-primed macrophages maintained their capacity to restrict *Mtb* replication at long-term post-vaccination.

DISCUSSION

Pulmonary BCG delivery is a topic a renewed interest in terms of its feasibility for use in clinic and its potential ability to confer a more specific and durable local protection in lungs against pulmonary TB. A recent clinical study of pulmonary BCG vaccination in healthy adult volunteers reported no major safety issues following vaccine administration with a bronchoscope (*29*). In addition, two clinical trials conducted by University of Oxford to evaluate safety and immunogenicity of BCG by the aerosol route in UK adults were recently completed (NCT02709278 and NCT03912207), with no major safety issues reported to date. From the perspective of protective efficacy, robust data in both mice and guinea pigs indicates improved protection conferred by intranasal BCG in comparison to subcutaneous BCG (*5, 6*). More recently, it was demonstrated that pulmonary BCG could prevent not only TB disease, but also TB infection in non-human primates (*7*). However, immunological mechanisms behind this protective effect are not completely understood, and the available studies focused on adaptive mucosal responses with little data about the interaction and modulation of lung myeloid populations by BCG.

AMs have been described as to represent a permissive population for *Mtb* replication, as has been reported for early stages of infection (*8*). According to our data, a relevant question should be why would virulent mycobacteria have evolved to acquire the ability to escape from this cellular niche and spread into other cellular subsets? One plausible explanation could be that naïve AMs but not activated AMs represent an *Mtb* permissive reservoir. A previous study showed that *in vivo* mycobacterial infection induced transcriptomic reprogramming in AMs shortly after infection, which was triggered by the NRF2 transcription factor and led to the acquisition of a pro-inflammatory phenotype (*21*). In addition, a recent publication describing lung cellular populations associated with active or latent TB in non-human primates showed a strong

correlation between high levels of AMs and infection control, whereas AMs are nearly absent in individuals with active TB (*30*). In agreement with these studies, we observed upregulation of activation markers in AMs from *Mtb*-infected mice compared with uninfected controls, and AMs expressed molecules with bactericidal functions including iNOS. At the time we detected activated AMs, only a small fraction of *Mtb* bacilli were contained inside these cells. These findings suggest that *Mtb* bacilli are under pressure to escape from naïve AMs before this cellular subset acquires TB-restrictive attributes. In the case of attenuated BCG, these bacilli appear to have lost the ability to escape from AMs upon infection and would likely be contained within these cells during cellular activation, which could contribute to the progressive clearance of BCG.

Our data indicate that pulmonary BCG induces global activation of both infected and non-infected macrophages. As a result, AMs from i.n. BCG-immunized mice that encounter *Mtb* upon pulmonary infection are already activated, which appears to have crucial consequences for the subsequent infection process. One of the most remarkable effects is the disruption of bacterial dissemination dynamics into bystander populations, including neutrophils and recruited IMs, which correlates with a substantial bacterial load reduction. This observation, together with the lower efficacy of attenuated BCG to leave AMs and colonize other cellular subsets, suggests the importance of bacterial spread dynamics for TB infection progression. Several other studies have shown neutrophil association with uncontained TB in animal models (*13, 14*), as well as active TB in humans (*12*). In contrast, our study showed that neutrophil depletion following *Mtb* challenge did not lead to a reduction of TB infection at least in terms of lung CFU, which may be due to incomplete neutrophil depletion. This cause is unlikely as our results showed a substantial reduction of *Mtb*-containing neutrophils, and we should have detected a measurable reduction of lung CFU mediated by neutrophils if they served as a

cellular reservoir for bacterial replication. It is more likely that neutrophils contribute to TB progression in a different way (*31, 32*). In this regard, we detected a decrease of MHCII expression in IMs from neutrophil-depleted mice, suggesting a possible role of neutrophils for optimal macrophage activation. A previous study described that infra-activated recruited IMs can represent a permissive niche for *Mtb* replication (*11*). This could explain the lack of CFU reduction observed in our experiments. Our data also demonstrated that in the absence of neutrophils, *Mtb* preferentially colonized IMs, indicating that virulent mycobacteria can escape from AMs regardless of the neutrophils' absence. This situation is different to which we observed in BCG pulmonary-vaccinated mice, in which *Mtb* was mainly restricted to AMs. This result supports our hypothesis that activated AMs are a TB restrictive population, with a strong capacity to contain the infection, and the escape of *Mtb* from AMs might represent a key virulence step.

It has been speculated that the success of *Mtb* in colonizing the lungs is due to delayed development of an effective cellular response prior to pathogen entry in the airways (*33*). During this time, non-activated AMs containing *Mtb* bacilli migrate to lung parenchyma and allow bacterial replication and dissemination, which critical for the establishment of infection (*8*). Replication control by the host correlates with migration of antigen-specific $CD4^+$ T cells to the lungs that had been activated in the draining lymph nodes (*34*). In the case of subcutaneous BCG immunization, the timing between bacterial encounter and the generation of the cellular response is reduced by vaccination, but there is a window in which bacteria can replicate and establish infection in the absence of cell-mediated immune responses (*33*). Reduction of this window has been shown to be a promising strategy to increase vaccine protective efficacy (*35*). Our data with i.n. BCG vaccination indicates that virulent mycobacteria are internalized by a TB restrictive cellular subset at early times of infection, and the window of opportunity for *Mtb* to

replicate properly and reach a critical bacterial load or disseminate towards permissive cellular subsets is dramatically reduced. This could explain an observation in NHP in which pulmonary BCG prevented TB infection in an ultra-low-dose repetitive challenge model, suggesting the induction of sterilizing immunity (*7*).

Our results indicate that BCG-activated AMs can contain TB infection in the absence of $CD4^+$ T cells when these cells are depleted during challenge phase. However, $CD4^+$ T cells are needed during vaccination phase to trigger protective macrophage activation. These results indicate that vaccine-triggered adaptive immunity is crucial for macrophage activation. However, once activated, macrophages can contain the infection, even preventing TB-induced mouse mortality, regardless of the presence or absence of T cells. It is highly probable that the contribution of T cells to AM activation is based on the supply of IFN-γ (*24*). In the case of BCG, $CD4^+$ T cells are the major contributors of IFN-γ, with an apparently dispensable contribution made by $CD8^+$ T cells. In contrast, a previous study using respiratory adenovirus delivery described the requirement of CD8+ T cells as IFN-γ producers and AMs activation inducers (*24*). The divergence between studies could be explained by the hypothesis that local IFN-γ production by adaptive lymphocytes is needed to induce macrophage activation, but the source of interferon depends on the primary stimulus. Viruses tend to induce $CD8^+$ T cell activation, but $CD4^+$ T cells are typically the source of IFN-γ upon exposure to intracellular mycobacteria like BCG, which we confirmed in our study.

Trained immunity has been described as the ability of innate immune cells to display a memory-like response similar to adaptive lymphocytes (*36*). BCG has been identified as a strong inducer of trained immunity in peripheral monocytes (*28*), as well as in myeloid precursors from the bone marrow following intravenous administration (*27*). However, as reviewed in a recent publication (*26*), the behaviour of innate immune cells

after receiving a primary stimulus can lead to different phenotypes caused by differentiation, tolerance and priming, in addition to responses associated with trained immunity. The trained phenotype is characterized by the return of the cellular immunological activation to a basal level following elimination of the primary stimulus, and epigenetic modifications remain that make cells respond more efficiently to respond to secondary stimuli. In the case if the priming process, the primary stimulus changes the functional state of these cells, and their immune status does not return to basal levels before the secondary stimulus or infection. In our long-term experiments, the immunological status of AMs after BCG clearance did not return to basal levels as MHCII and CD86 expression was still elevated. Inflammatory genes including *Irf8* were also upregulated in i.n. BCG-activated AMs following vaccine clearance. Considering our current understanding of trained immunity (*26*), it is not clear whether BCG induces training or priming on AMs following local vaccination. However, and independently of this classification, our results demonstrate that BCG-activated AMs have the capacity to trigger an enhanced response against a subsequent challenge. This study reports the ability of BCG to induce a memory-like response in AMs and, importantly, the capacity of long-term BCG-activated AMs to respond efficiently upon a challenge with *Mtb*. The presence of infiltrated IMs and neutrophilia disappeared when BCG was removed. From the safety perspective, this would indicate that pulmonary BCG vaccination is not inducing chronic inflammation that could lead to harmful collateral consequences.

A significant limitation of our results to be translated into a more relevant scenario might rest on the route of vaccination chosen to deliver BCG into the lungs. It is unlikely that intranasal route might be authorized for live vaccine administration in clinic, due to safety concerns. Conversely, aerosol delivery could be more probable, and indeed BCG aerosolized with clinical nebulizers is already under early clinical evaluation. Since it is

not feasible to test this type of devices in the mouse model, it would be important to characterize myeloid populations in human studies (or non-human primates), to confirm the role of AMs in protection following BCG aerosol administration.

Researchers working on TB vaccines have been trying to identify immunological parameters based on adaptive cellular responses that correlate with vaccine-induced protection, but there is growing interest in the role of non-canonical responses for protection against TB. Antibodies, NK cells, or IFN-γ-negative T cells have been shown to be important for natural protection against TB (*37-39*), and innate defences have been associated with early elimination of TB infection (*40*). Here we have shown that it is possible to modulate lung macrophage activation through local BCG vaccination, thus demonstrating that the induction of long-term immunity on tissue-resident macrophages could represent a viable approach for experimental vaccines.

METHODS

Study design

This study aimed to analyze the contribution of alveolar macrophages to tuberculosis protection induced by the vaccine BCG delivered by pulmonary route. Groups of mice were randomly distributed in groups of 3-6 animals per cage in each experiment. The number of biological replicates and number of repetitions for each experiment are indicated in figure legends. Results were not blinded for analysis.

Ethics statement

Experimental work was conducted in agreement with European and national directives for protection of experimental animals and experimental procedures were approved by the Ethics Committee for Animal Experiments of University of Zaragoza

(PI46/18, PI33/15 PI50/14). Male and female mice between the ages of 8 to 10 weeks were used for all the experiments.

Mice

C57BL/6JR mice were purchased from Janvier Biolabs. Csf1r-eCFP x LysM-GFP mice were obtained at the animal facilities from the IPBS (Toulouse, France), by crossing the Csf1r-eCFP (*18*) and LysM-GFP (*19*) strains. All mice were housed and maintained in specific pathogen-free conditions and observed for any sign of disease in the facilities of Centro de Investigación de Encefalopatías y Enfermedades Transmisibles Emergentes (CIEETE, Zaragoza, Spain, reference ES 50 297 0012 009) and *Centro de Investigaciones Biomédicas de Aragón* (CIBA, Zaragoza, Spain, reference ES 50 297 0012 011).

Bacterial strains

Mycobacterial strains used in this study were grown at 37°C in Middlebrook 7H9 broth (BD Difco) supplemented with 0.05% Tween 80 (Sigma) and 10% Middlebrook albumin dextrose catalase enrichment (ADC; BD Biosciences) or on solid Middlebrook 7H10 agar (BD Difco) supplemented with 10 % ADC (BD Biosciences). When required, medium was supplemented with 20 μg/ml of kanamycin. GFP-expressing strains of H37Rv, BCG Pasteur and BCG::RD1 (a kind gift from Roland Brosch, Institute Pasteur Paris, France) were generated by transformation with the replicative plasmid pJKD6 (a kind gift from Luciana Leite, Butantan Institute, Brazil). This plasmid carries de *gfp* gene under the control of a strong promoter generated through error-prone PCR of the PL5 promoter from the mycobacteriophage L5 (*41*).

Bacterial suspensions for intranasal or subcutaneous vaccinations or intranasal infections were prepared in PBS from quantified glycerol stock solutions.

Intranasal infection and vaccine administration

Our experience studying intranasal (i.n.) delivery of virulent and attenuated strains as route of pulmonary administration indicates that this route is comparable to intratracheal delivery, and we selected i.n. delivery for infection with H37Rv::*gfp*. The animals were anesthetized and i.n. administration was performed with two instillations of 20 µl (one per nostril) of the bacterial suspension prepared in PBS. Infection doses were optimized based on the number of infected cells needed for subsequent analysis of lung infected populations by flow cytometry at each time point. The H37Rv::*gfp* infection doses were defined as 10^6 CFUs for day 1 and day 7, 10^5 CFUs for day 13, and 10^4 CFUs for day 24.

Vaccination was performed with 10^6 CFUs of BCG Pasteur or BCG Pasteur::*gfp* by the i.n. or s.c. route. For s.c. vaccination, mice were injected s.c. with 100 µl of bacterial suspension prepared in PBS. For protection experiments, mice immunized with 10^6 CFUs of BCG Pasteur by i.n. or s.c. routes and challenged i.n. with H37Rv::*gfp* at the indicated time points post-vaccination.

Lung single cell suspension Preparation

Lungs were aseptically removed and homogenized in HEPES buffer (HEPES 10 mM, NaCl, 150 mM, KCl 5 mM, $MgCl_2$ 1 mM, $CaCl_2$ 1.8 mM pH 7,4) containing DNaseI (AppliChem) 40 IU/ml and Collagenase D (Roche) 2 mg/ml using a GentleMacs dissociator (Miltenyi Biotec) according to manufacturer instructions. Lungs were incubated at 37 ºC for 30 minutes and further homogenized with the GentleMacs dissociator. The homogenates were filtered through a 70 µm cell strainer (MACS SmartStainers, Miltenyi Biotec) and centrifuge at 1,500 rpm for 5 min. Red blood cells were lysed using red blood cell lysing Buffer (Sigma-Aldrich) and cells were pelleted and resuspended in RPMI culture medium (Gibco) for antibody staining.

Antibody staining and Flow Cytometry

A list of antibodies used for cellular characterization is described in the table S1. Lung single cell suspensions were plated in U-bottom 96-well plates and incubated for 15 minutes at 4 ºC with FcR blocking reagent (Miltenyi Biotec). Surface staining was performed for 20 min at 4º C using different combinations of antibodies to define myeloid lung cell populations and macrophage activation status. Then, cells were washed and fixed with 4% paraformaldehyde for 30 minutes.

For intracellular staining of iNOS and IFNγ, cells were fixed and permeabilized after surface staining with FoxP3 staining set (Miltenyi Biotec) for 30 minutes at 4 ºC, washed and incubated with anti-mouse iNOS APC (Miltenyi Biotec) or anti-mouse IFNγ-APC (Miltenyi Biotec) for 1 hour at room temperature.

For intracellular staining of Ki67, cells were fixed and permeabilized after surface staining with FoxP3/ transcription factor staining buffer set (eBiosciences) for 30 minutes at 4 ºC, washed and incubated with anti-mouse Ki67-percCPVio-700 (Miltenyi Biotec) for 1 hour at room temperature.

Cells were acquired using a Gallios flow cytometer (Beckman Coulter) and the results were analysed using Weasel Software.

Lung alveolar macrophages were defined as $CD45^{+}CD64^{+}CD11c^{high}SiglecF^{+}$, interstitial macrophages as $CD45^{+}CD64^{+}CD11c^{dim}SiglecF^{-}$ and neutrophils as $CD45^{+}Ly6G^{+}CD11c^{-}CD11b^{+}SiglecF^{-}$. Macrophage activation status was assessed using anti-mouse MHCII, CD86 and iNOS.

CD45 labelling

For intravenous CD45 labeling, mice were i.v. injected with 2 µg of CD45-percPVio700 (Miltenyi) 10 minutes prior to sacrifice.

IFN-γ determination

For intracellular staining of IFN-γ producing T cells, lung single cell suspensions were incubated overnight in U-bottom 96-well plates with 10 µg/ml of PPD at 37 ºC and 5% of CO2. Brefeldin A (Invitrogen) was added and cells were incubated for 4 hours at 37ºC and 5% CO_2 prior to intracellular staining.

For total IFN-γ determination in lungs *ex vivo*, lungs were homogenized in 1 ml of H_2O using a GentleMacs dissociator (Miltenyi Biotec) and incubated overnight in 24-well plates at 37 ºC and 5% CO_2. Supernatants were recovered, and IFN-γ was quantified by ELISA using an IFN-γ detection kit (Mabtech Biotech) according to manufacturer instructions.

Bacterial burden determination

To analyze bacterial burden, lungs were homogenized in 1 ml of ddH_2O using a GentleMacs dissociator (Miltenyi Biotec) and CFUs were determined by plating serial dilutions on solid Middlebrook 7H10 medium (BD Difco) supplemented with 10% Middlebrook ADC enrichment (BD).

Lethal challenge with *Streptococcus pneumoniae*

Mice were inoculated by the intranasal route with 50 µl containing 1×10^4 CFU/mouse of 957/13 strain of serotype 3. This is a *S. pneumoniae* clinical isolate from a 57 years old patient who suffered community-acquired bacterial pneumonia. Bacterial levels in blood, were determined from each infected mouse at 24 h, 48 h, and 72 h post infection from a 6 µl sample of blood collected from the tail vein. Mice were monitored for a period of 7 days. Experiments were repeated twice using 5 mice in each group, and results were expressed as $\log_{10}$ CFU/ml of bacteria recovered from the blood.

***In vivo* depletion**

To deplete CD4+ and CD8+ T cells, mice were injected intraperitoneally one week prior to H37Rv::*gfp* challenge or BCG Pasteur vaccination with 300 µg of anti-mouse CD4 (clone GK1.5, BioXCell) or anti-mouse CD8α (clone 2.43, BioXCell). Repeated doses of 100 µg of of anti-CD4 or 150 µg of anti-CD8α were administered i.p. two times a week to achieve continuous depletion.

For neutrophil depletion, mice were injected i.p. with 100 µg of anti-Ly6G (clone 1A8, BioXCell), alternating with 100 µg of anti-rat-IgGK (clone MAR 18.5, BioXCell) (*20*). Treatment was started prior to H37Rv::*gfp* challenge and was maintained during the course of the experiment.

Microscopy

Lungs of Csf1r-eCFP x LysM-GFP infected mice were harvested and fixed in PFA 4% in PBS for 48 hours. After fixation, lungs were submitted to a sucrose gradient (10%, 20% and 30% in PBS) followed by embedding in OCT (Tissue-Tek) and freezing in a cold (-20°C) bath. Samples were kept at -80°C until used. Cryosectioning was performed in a Leica Cryostat and several 30µm sections were made for each lung. Lung sections were washed three times in cell stain buffer (BD Biosciences) and mounted on ProLong Glass Antifade (ThermoFisher) with a coverslip. 3D image stacks were acquired on a Zeiss LSM710 NLO confocal microscope using a Zeiss 20x objective NA=0.8 in sequential acquisition mode to minimize crosstalk between fluorescent proteins, in particular CFP and GFP. Image analysis was performed in Imaris (Bitplane) for the creation of representative images and ImageJ (NIH, USA) plugin Cell counter to manually quantify the % of infected neutrophils per image.

Gene expression analysis

Lung single cell suspensions were obtained from 2- or 7-months vaccinated mice, and AMs were purified as $CD45^{+}CD64^{+}CD11c^{+}SiglecF^{+}$ cells using a Sony SH-800S Cell Sorter. RNA was obtained from sorted AMs using RNeasy micro kit (QIAGEN). Sorted cells were directly collected in RLT plus lysis buffer (provided by RNeasy micro kit) and RNA purification was performed according to manufacturer instructions. cDNA libraries were constructed using Prime Script RT Master Mix (Takara) according to manufacturer instructions. TB Green Premix ExTaqTM (Tli RNase H Plus) (Takara) was used for qRT-PCR reaction. Each reaction was performed in triplicate and qRT-PCR were carried out in StepOne Plus Real Time PCR System (Applied Biosystems). Primer sequences are detailed in table S2.

Quantification and statistical analysis

Flow cytometry data were analysed using Weasel software (version 3.0.2) and presented as mean ± SD. GraphPad Prism software (version 6) was used for graphical representation and statistical analysis. All tests applied were two-sided. For comparisons between two groups, analysis was done by unpaired t-student test. For more than two groups, we used one-way ANOVA or two-way ANOVA for one or two variable analysis, respectively. Survival was analyzed by the Log-rank (Mantel-Cox) test. A p value of < 0.05 was considered significant (ns: non-significant, *$p < 0.05$, **$p < 0.01$,***$p < 0.001$, ****$p < 0.0001$).

LIST OF SUPPLEMENTARY MATERIALS

REFERENCES

1. WHO, WHO | Global tuberculosis report 2019. (2020).
2. F. B. Garner, C. A. Meyer, D. S. White, A. Lipton, Aerosol BCG treatment of carcinoma metastatic to the lung: a phase I study. *Cancer* **35**, 1088-1094 (1975).
3. S. R. Rosenthal, J. T. McEnery, N. Raisys, Aerogenic BCG vaccination against tuberculosis in animal and human subjects. *J Asthma Res* **5**, 309-323 (1968).
4. N. Aguilo *et al.*, Pulmonary Mycobacterium bovis BCG vaccination confers dose-dependent superior protection compared to that of subcutaneous vaccination. *Clin Vaccine Immunol* **21**, 594-597 (2014).
5. M. Lagranderie *et al.*, BCG-induced protection in guinea pigs vaccinated and challenged via the respiratory route. *Tuber Lung Dis* **74**, 38-46 (1993).
6. N. Aguilo *et al.*, Pulmonary but Not Subcutaneous Delivery of BCG Vaccine Confers Protection to Tuberculosis-Susceptible Mice by an Interleukin 17-Dependent Mechanism. *J Infect Dis* **213**, 831-839 (2016).
7. K. Dijkman *et al.*, Prevention of tuberculosis infection and disease by local BCG in repeatedly exposed rhesus macaques. *Nat Med* **25**, 255-262 (2019).
8. S. B. Cohen *et al.*, Alveolar Macrophages Provide an Early Mycobacterium tuberculosis Niche and Initiate Dissemination. *Cell Host Microbe* **24**, 439-446 e434 (2018).
9. L. Huang, E. V. Nazarova, S. Tan, Y. Liu, D. G. Russell, Growth of Mycobacterium tuberculosis in vivo segregates with host macrophage metabolism and ontogeny. *J Exp Med* **215**, 1135-1152 (2018).
10. M. Skold, S. M. Behar, Tuberculosis triggers a tissue-dependent program of differentiation and acquisition of effector functions by circulating monocytes. *J Immunol* **181**, 6349-6360 (2008).
11. L. R. Antonelli *et al.*, Intranasal Poly-IC treatment exacerbates tuberculosis in mice through the pulmonary recruitment of a pathogen-permissive monocyte/macrophage population. *J Clin Invest* **120**, 1674-1682 (2010).
12. M. P. Berry *et al.*, An interferon-inducible neutrophil-driven blood transcriptional signature in human tuberculosis. *Nature* **466**, 973-977 (2010).
13. A. Dorhoi *et al.*, Type I IFN signaling triggers immunopathology in tuberculosis-susceptible mice by modulating lung phagocyte dynamics. *Eur J Immunol* **44**, 2380-2393 (2014).
14. E. B. Eruslanov *et al.*, Neutrophil responses to Mycobacterium tuberculosis infection in genetically susceptible and resistant mice. *Infect Immun* **73**, 1744-1753 (2005).
15. A. J. Wolf *et al.*, Mycobacterium tuberculosis infects dendritic cells with high frequency and impairs their function in vivo. *J Immunol* **179**, 2509-2519 (2007).
16. J. I. Aguilo *et al.*, ESX-1-induced apoptosis is involved in cell-to-cell spread of Mycobacterium tuberculosis. *Cell Microbiol* **15**, 1994-2005 (2013).
17. A. S. Pym, P. Brodin, R. Brosch, M. Huerre, S. T. Cole, Loss of RD1 contributed to the attenuation of the live tuberculosis vaccines Mycobacterium bovis BCG and Mycobacterium microti. *Mol Microbiol* **46**, 709-717 (2002).
18. D. A. Ovchinnikov *et al.*, Expression of Gal4-dependent transgenes in cells of the mononuclear phagocyte system labeled with enhanced cyan fluorescent

protein using Csf1r-Gal4VP16/UAS-ECFP double-transgenic mice. *J Leukoc Biol* **83**, 430-433 (2008).
19. N. Faust, F. Varas, L. M. Kelly, S. Heck, T. Graf, Insertion of enhanced green fluorescent protein into the lysozyme gene creates mice with green fluorescent granulocytes and macrophages. *Blood* **96**, 719-726 (2000).
20. G. Boivin *et al.*, Durable and controlled depletion of neutrophils in mice. *Nat Commun* **11**, 2762 (2020).
21. A. C. Rothchild *et al.*, Alveolar macrophages generate a noncanonical NRF2-driven transcriptional response to Mycobacterium tuberculosis in vivo. *Sci Immunol* **4**, (2019).
22. R. J. W. Arts *et al.*, Immunometabolic Pathways in BCG-Induced Trained Immunity. *Cell Rep* **17**, 2562-2571 (2016).
23. J. Dominguez-Andres, S. Fanucchi, L. A. B. Joosten, M. M. Mhlanga, M. G. Netea, Advances in understanding molecular regulation of innate immune memory. *Curr Opin Cell Biol* **63**, 68-75 (2020).
24. Y. Yao *et al.*, Induction of Autonomous Memory Alveolar Macrophages Requires T Cell Help and Is Critical to Trained Immunity. *Cell* **175**, 1634-1650 e1617 (2018).
25. J. L. Delahaye *et al.*, Cutting Edge: Bacillus Calmette-Guerin-Induced T Cells Shape Mycobacterium tuberculosis Infection before Reducing the Bacterial Burden. *J Immunol* **203**, 807-812 (2019).
26. M. Divangahi *et al.*, Trained immunity, tolerance, priming and differentiation: distinct immunological processes. *Nat Immunol* **22**, 2-6 (2021).
27. E. Kaufmann *et al.*, BCG Educates Hematopoietic Stem Cells to Generate Protective Innate Immunity against Tuberculosis. *Cell* **172**, 176-190 e119 (2018).
28. J. Kleinnijenhuis *et al.*, Bacille Calmette-Guerin induces NOD2-dependent nonspecific protection from reinfection via epigenetic reprogramming of monocytes. *Proc Natl Acad Sci U S A* **109**, 17537-17542 (2012).
29. M. Davids *et al.*, A Human Lung Challenge Model to Evaluate the Safety and Immunogenicity of PPD and Live BCG. *Am J Respir Crit Care Med*, (2019).
30. E. Esaulova *et al.*, The immune landscape in tuberculosis reveals populations linked to disease and latency. *Cell Host Microbe* **29**, 165-178 e168 (2021).
31. J. Pedrosa *et al.*, Neutrophils play a protective nonphagocytic role in systemic Mycobacterium tuberculosis infection of mice. *Infect Immun* **68**, 577-583 (2000).
32. C. T. Yang *et al.*, Neutrophils exert protection in the early tuberculous granuloma by oxidative killing of mycobacteria phagocytosed from infected macrophages. *Cell Host Microbe* **12**, 301-312 (2012).
33. A. M. Cooper, Cell-mediated immune responses in tuberculosis. *Annu Rev Immunol* **27**, 393-422 (2009).
34. A. J. Wolf *et al.*, Initiation of the adaptive immune response to Mycobacterium tuberculosis depends on antigen production in the local lymph node, not the lungs. *J Exp Med* **205**, 105-115 (2008).
35. K. L. Griffiths *et al.*, Targeting dendritic cells to accelerate T-cell activation overcomes a bottleneck in tuberculosis vaccine efficacy. *Nat Commun* **7**, 13894 (2016).
36. M. G. Netea, J. Quintin, J. W. van der Meer, Trained immunity: a memory for innate host defense. *Cell Host Microbe* **9**, 355-361 (2011).

37. L. L. Lu *et al.*, A Functional Role for Antibodies in Tuberculosis. *Cell* **167**, 433-443 e414 (2016).
38. L. L. Lu *et al.*, IFN-gamma-independent immune markers of Mycobacterium tuberculosis exposure. *Nat Med* **25**, 977-987 (2019).
39. R. Roy Chowdhury *et al.*, A multi-cohort study of the immune factors associated with M. tuberculosis infection outcomes. *Nature* **560**, 644-648 (2018).
40. S. A. Khader *et al.*, Targeting innate immunity for tuberculosis vaccination. *J Clin Invest* **129**, 3482-3491 (2019).
41. A. I. Kanno *et al.*, New Recombinant Mycobacterium bovis BCG Expression Vectors: Improving Genetic Control over Mycobacterial Promoters. *Appl Environ Microbiol* **82**, 2240-2246 (2016).

ACKNOWLEDGEMENTS

We thank the Scientific and Technical Services from Instituto Aragonés de Ciencias de la Salud and Universidad de Zaragoza for their assistance. We acknowledge the help of the TRI-IPBS Imaging and Anexplo Core Facilities, members Genotoul, as well as Florence Levillain for preparing mycobacteria for microscopy experiments.

FUNDING

Supported by Spanish Ministry of "Ciencia, Innovación y Universidades" [grant number RTI2018-097625-B-I00]; and "Gobierno de Aragón-Fondo Europeo de Desarrollo Regional (FEDER) 2014-2020: Construyendo Europa Desde Aragón". The funders had no role in study design, data collection and analysis, decision to publish or preparation of the manuscript.

AUTHORS CONTRIBUTION

J.D.A., J.Y., A.P., C.M. and N.A. designed the experiments. C.M. and N.A supervised the study. E.M., R.T., C.G., E.M., F.M., S.U., A.B.G., M.D. and F.G.D. performed the experiments. M.M. and J.B. shared BSL3 animal facilities. E.M., D.M., M.M., J.B., A.A., J.D.A, A.P., C.M. and N.A. wrote the manuscript.

COMPETING INTERESTS STATEMENT

Raquel Tarancón, Elena Mata, Santiago Uranga, Dessislava Marinova, Carlos Martín and Nacho Aguiló are co-inventors of the patent "Therapeutic efficacy by pulmonary delivery of live attenuated mycobacteria" held by the University of Zaragoza.

DATA AVAILABILITY STATEMENT

Data and materials available on request from the authors.

789 **FIGURES**

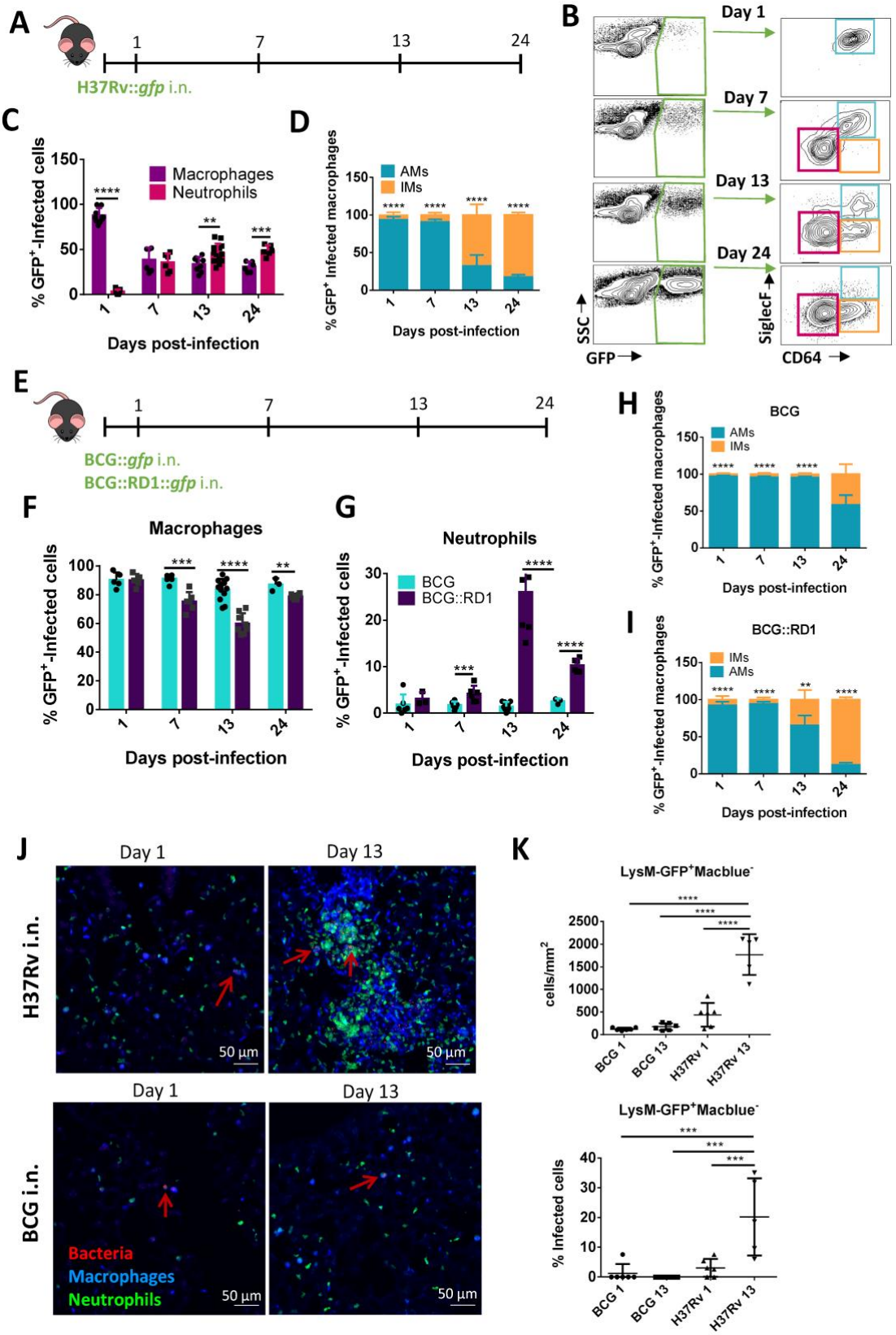

790

Fig. 1. Differential cell-to-cell dissemination patterns between virulent and attenuated strains. A. Schema of respiratory *Mtb* infection. Adult C57BL/6 mice were infected intranasally (i.n.) with GFP-tagged *Mtb* (H37Rv::*gfp*). **B.** Representative dot plots showing *Mtb*-infected cells at days 1, 7, 13 and 24 post-infection, and proportions of GFP positive-gated populations determined by CD64 and SiglecF markers analysis. Boxes correspond to alveolar macrophages (AMs) (blue), interstitial macrophages (IMs) (orange) and neutrophils (pink). **C.** Frequencies of *Mtb*-infected macrophages and neutrophils. **D.** Frequencies of *Mtb*-infected AMs and IMs. **E.** Schema of i.n. administration of GFP-tagged BCG and BCG::RD1 in mice. **F.** Frequencies of BCG and BCG::RD1-infected macrophages. **G.** Frequencies of BCG and BCG::RD1-infected neutrophils. **H.** Frequencies of BCG-infected AMs and IMs I. Frequencies of BCG::RD1-infected AMs and IMs. **J.** Maximum intensity projection of confocal microscopy stacks of lung tissue sections from Csf1r-eCFP x LysM-GFP infected mice at day 1 and 13 post-infection. Neutrophils are GFP positive CFP negative whereas macrophages and monocytes are CFP positive. Red arrows highlight examples of infected cells. **K.** Quantification of total (upper panel) and infected (lower panel) neutrophils from confocal microscopy images. (**C**-**H**) Pooled data from two independent experiments **(**n = 6 mice/group). Graphs are presented as mean ± SD. **p < 0.01; *** < 0.001; **** < 0.0001 by multiple unpaired t-student test (**C, D, F, G, H**) and one-way ANOVA with Bonferroni post-test (**K**).

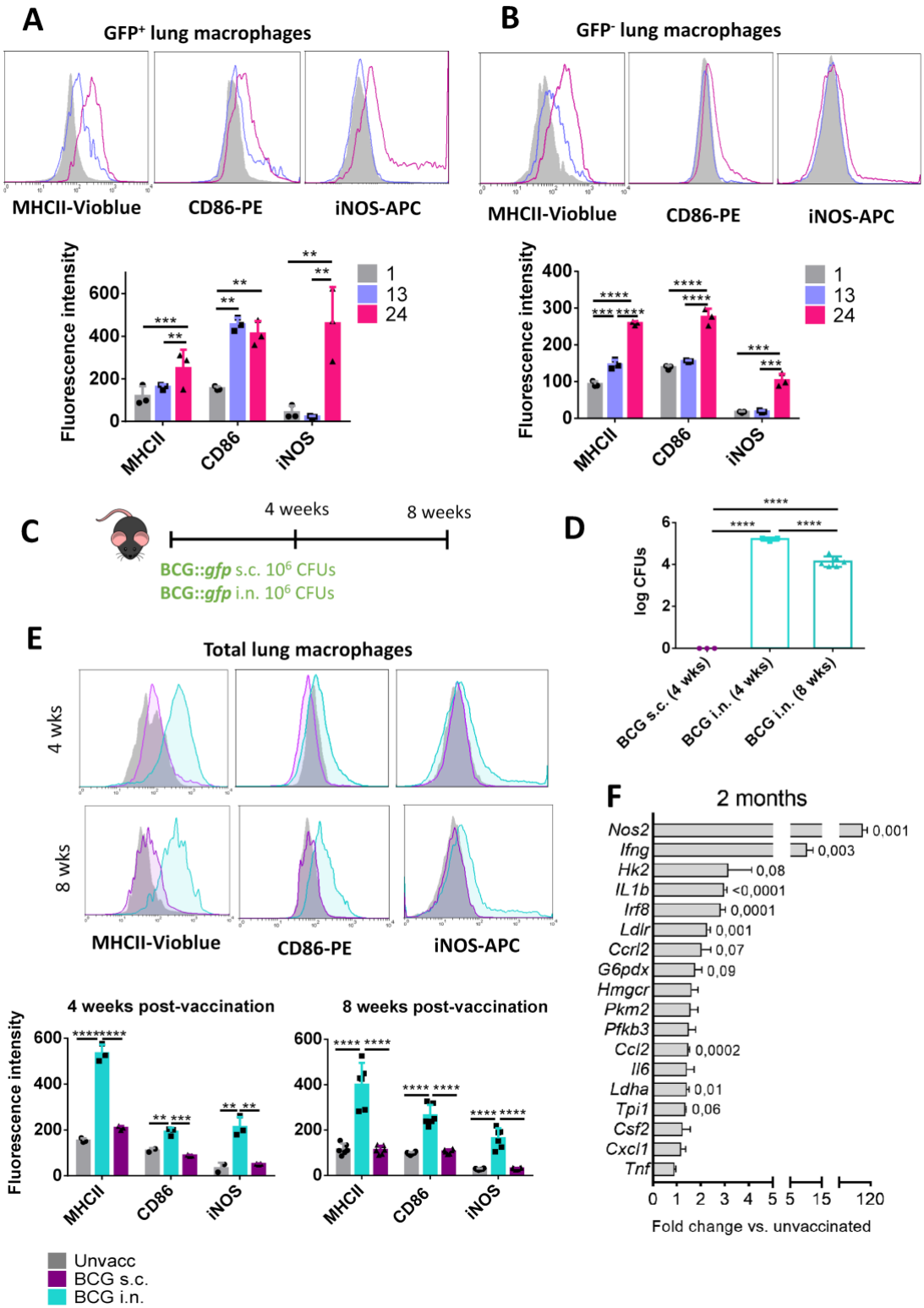

Fig. 2. Presence of BCG in the lung triggers lung macrophage activation. A. Representative histograms and fluorescence intensity of MHCII, CD86 and iNOS expression gated on BCG-infected macrophages (GFP+) at days 1 (grey), 13 (blue) and 20 (pink) post-inoculation of adult C57BL/6 mice with GFP-tagged BCG. **B.** MHCII,

CD86 and iNOS expression by non-infected macrophages (GFP-). **C.** Schema of GFP-tagged BCG vaccination of mice by intranasal (i.n.) and subcutaneous (s.c.) routes. **D.** BCG CFUs in lungs at 4- and 8-weeks post-vaccine administration. **E.** MHCII, CD86 and iNOS expression by total lung macrophages from s.c. BCG (purple) and i.n. BCG (blue) groups or unvaccinated (grey) mice **F.** Relative gene expression of sorted AMs from BCG i.n. vaccinated mice 8 weeks post-vaccination. Data are representative of two independent experiments (n = 6 mice/group). Graphs are presented as mean ± SD. **p < 0.01; ***p < 0.001; ****p < 0.0001 by one-way ANOVA with Bonferroni post-test (**A, B, D, E, F**).

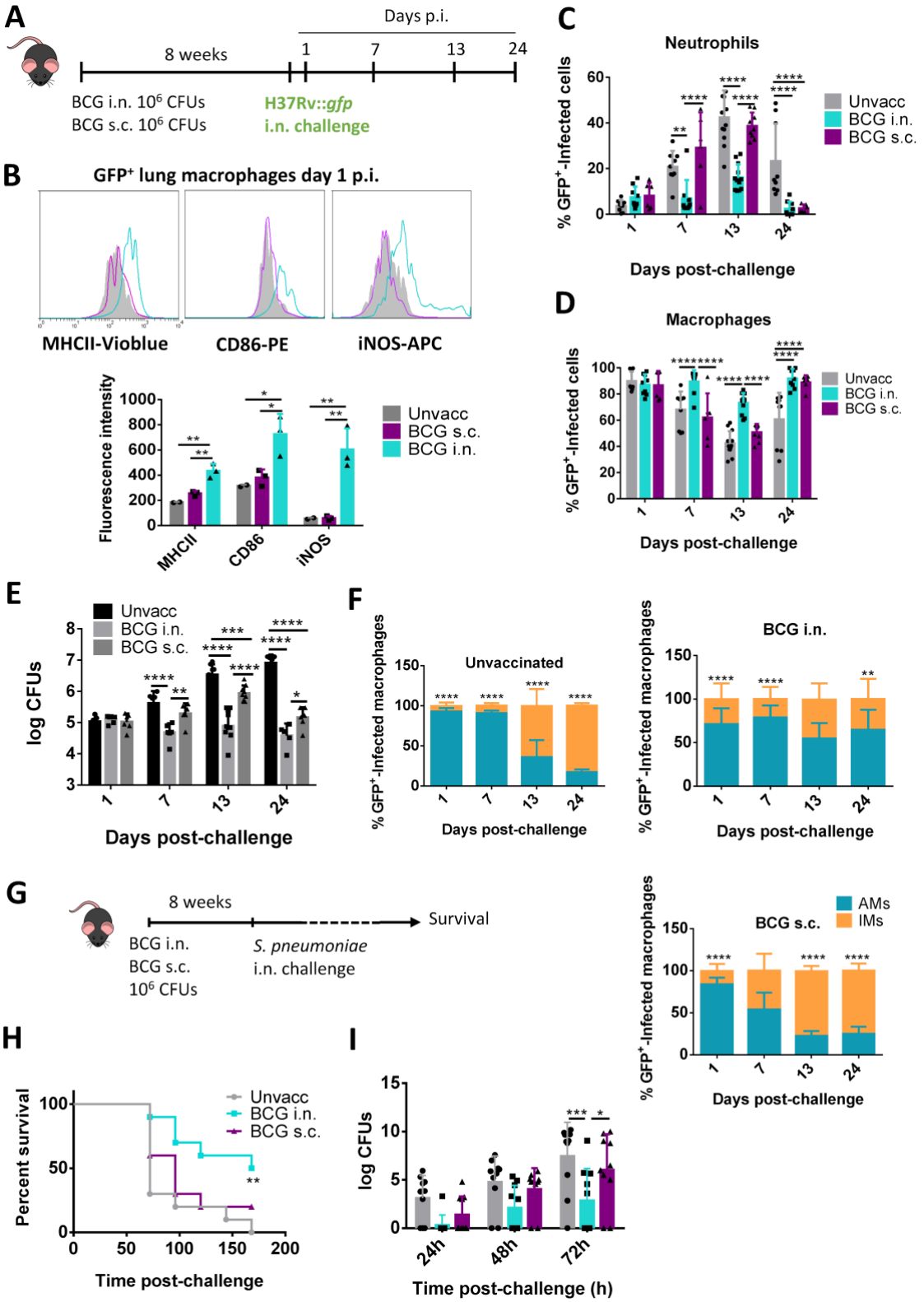

826

827 **Fig. 3. Lung macrophages from pulmonary, but not subcutaneous, BCG-vaccinated**

828 **mice are protective against *Mtb*. A.** Schema of i.n. and s.c. vaccination of mice with

829 non-fluorescent BCG and subsequent i.n. challenge with GFP-expressing H37Rv

measured in days post-infection (p.i.). **B.** Representative histograms and fluorescence intensity of MHCII, CD86 and iNOS expression gated on H37Rv-infected macrophages at day 1 post-challenge, in unvaccinated (grey) s.c. BCG-vaccinated (purple) and i.n. BCG-vaccinated (blue) mice. **C.** Frequencies of *Mtb*-infected neutrophils in unvaccinated (grey), s.c. BCG-vaccinated (purple) and i.n. BCG-vaccinated (blue) mice. **D.** Frequencies of *Mtb*-infected macrophages in unvaccinated (grey), s.c. BCG-vaccinated (purple) and i.n. BCG-vaccinated (blue) mice. **E.** *Mtb* bacterial loads in lungs in unvaccinated, s.c BCG-vaccinated and i.n. BCG-vaccinated mice. **F.** Frequencies of *Mtb*-infected AMs and IMs in unvaccinated, s.c. BCG-vaccinated and i.n. BCG-vaccinated mice. **G.** Schema of i.n. and s.c. vaccination of mice with BCG and subsequent i.n. challenge with *S. pneumoniae*. **H.** Survival curve of unvaccinated, s.c. BCG-vaccinated and i.n. BCG-vaccinated mice following *S. pneumoniae* challenge. **I.** *S. pneumoniae* bacterial loads in blood in unvaccinated, s.c. BCG-vaccinated and i.n. BCG-vaccinated mice at 24, 48 and 72h post-infection. **(B)** Data are representative of two independent experiments (n=3 mice/group). (**C-F)** Pooled data from two independent experiments (n = 6 mice/group). (**I**) Pooled data from two independent experiments (n = 4-5 mice/group). Graphs are presented as mean ± SD. *$p < 0.05$; **$p < 0.01$; ***$p < 0.001$; ****$p < 0.0001$ by one-way ANOVA with Bonferroni post-test (**B**) and two-way ANOVA with Bonferroni post-test (**C-I**). Survival was analyzed by the Log-rank (Mantel-Cox) test.

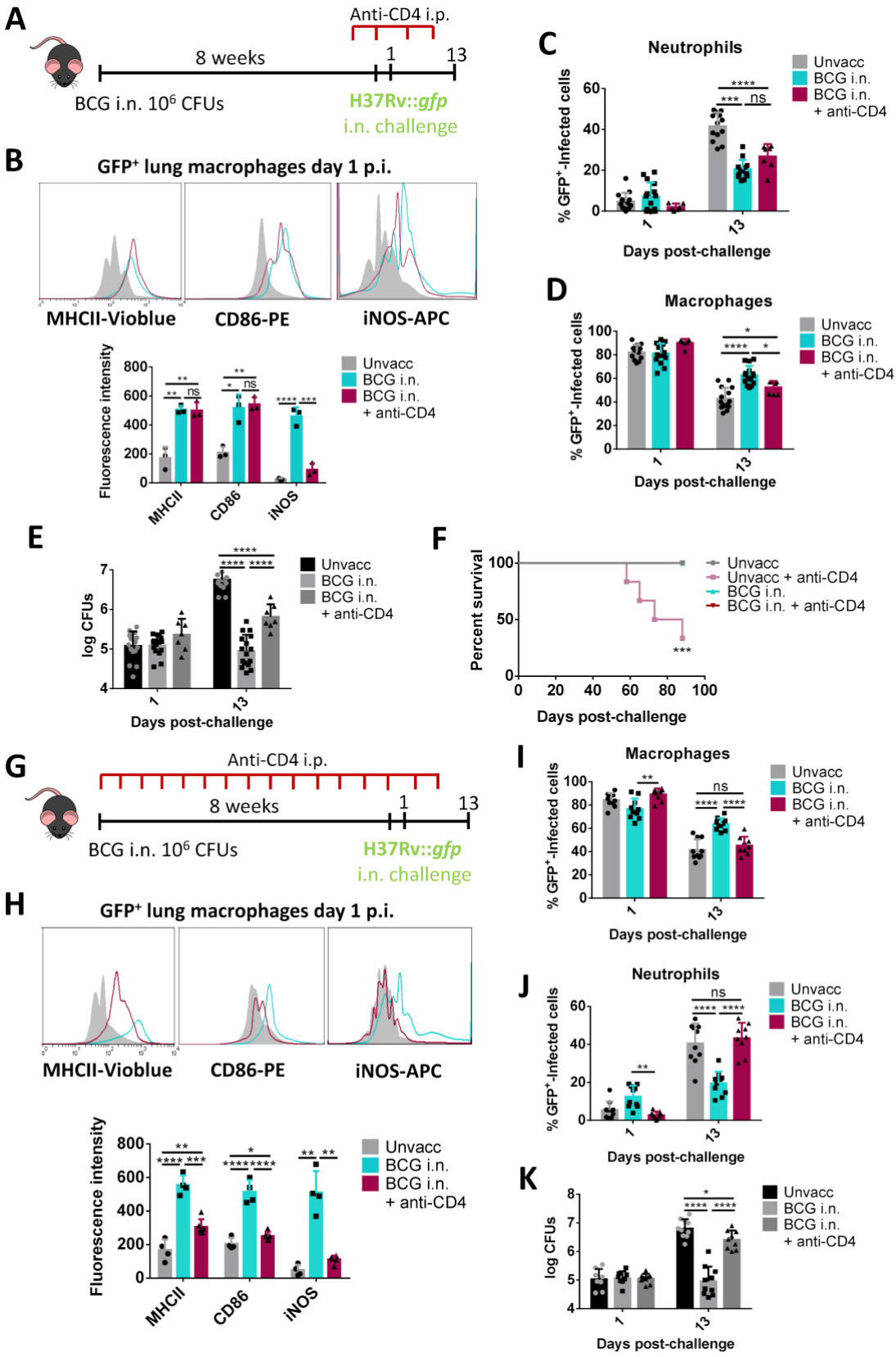

850

851 **Fig. 4. CD4+T cells contribute to vaccine-induced macrophage activation. A.** Schema

852 of i.n. vaccination with non-fluorescent BCG in mice, and subsequent i.n. challenge with

GFP-expressing H37Rv, with CD4+ T-cell depletion treatment by intraperitoneal (i.p.) administration of anti-CD4 neutralizing antibodies, starting 7 days prior to i.n. H37Rv challenge. **B.** Representative histograms and fluorescence intensity of MHCII, CD86 and iNOS expression gated on H37Rv-infected macrophages at day 1 post-challenge, in unvaccinated (grey), i.n. BCG-vaccinated (blue) and i.n. BCG-vaccinated CD4+ T cell-depleted (red) groups. **C.** Frequencies of *Mtb*-infected neutrophils in unvaccinated (grey), i.n. BCG-vaccinated (blue) and i.n. BCG-vaccinated CD4+cells-depleted (red) mice. **D.** Frequencies of *Mtb*-infected macrophages in unvaccinated (grey), i.n BCG-vaccinated (blue) and i.n. BCG-vaccinated CD4+ cell-depleted (red) mice. **E.** *Mtb* bacterial loads in lungs in unvaccinated, i.n. BCG-vaccinated, and i.n. BCG-vaccinated/CD4+ T cell-depleted mice. **F.** Survival curve using a low-dose *Mtb* challenge of 500 CFUs, and CD4+ T cell depletion starting by the challenge. **G.** Schema of i.n. vaccination of mice with non-fluorescent BCG, and subsequent i.n. challenge with GFP-expressing H37Rv, with intraperitoneal (i.p.) CD4+ T cell-depletion treatment, starting 7 days prior to i.n. BCG vaccination. **H.** Representative histograms and fluorescence intensity of MHCII, CD86 and iNOS expression gated on H37Rv-infected macrophages at day 1 post-challenge, in unvaccinated (grey), i.n. BCG-vaccinated (blue) and i.n. BCG-vaccinated CD4+ T cell-depleted (red) mouse groups. **I.** Frequencies of *Mtb*-infected macrophages in unvaccinated (grey), i.n. BCG-vaccinated (blue) and i.n. BCG-vaccinated, CD4+cell-depleted (red) mice. **J.** Frequencies of *Mtb*-infected neutrophils in unvaccinated (grey), i.n. BCG-vaccinated (blue) and i.n. BCG-vaccinated, CD4+ T cell-depleted (red) mice. **K.** *Mtb* bacterial loads in lungs of unvaccinated, i.n. BCG-vaccinated and i.n. BCG-vaccinated CD4+ T cell-depleted groups. Data are representative of two independent experiments (n = 6 mice/group). Graphs are presented as mean ± SD. ns, non-significant *$p < 0.05$; **$p < 0.01$; ***$p < 0.001$; ****$p < 0.0001$ by one-way ANOVA with

878 Bonferroni post-test (**B, H**), and two-way ANOVA with Bonferroni post-test (**C-F, I-K**).

879 Survival was analyzed by the Log-rank (Mantel-Cox) test.

880

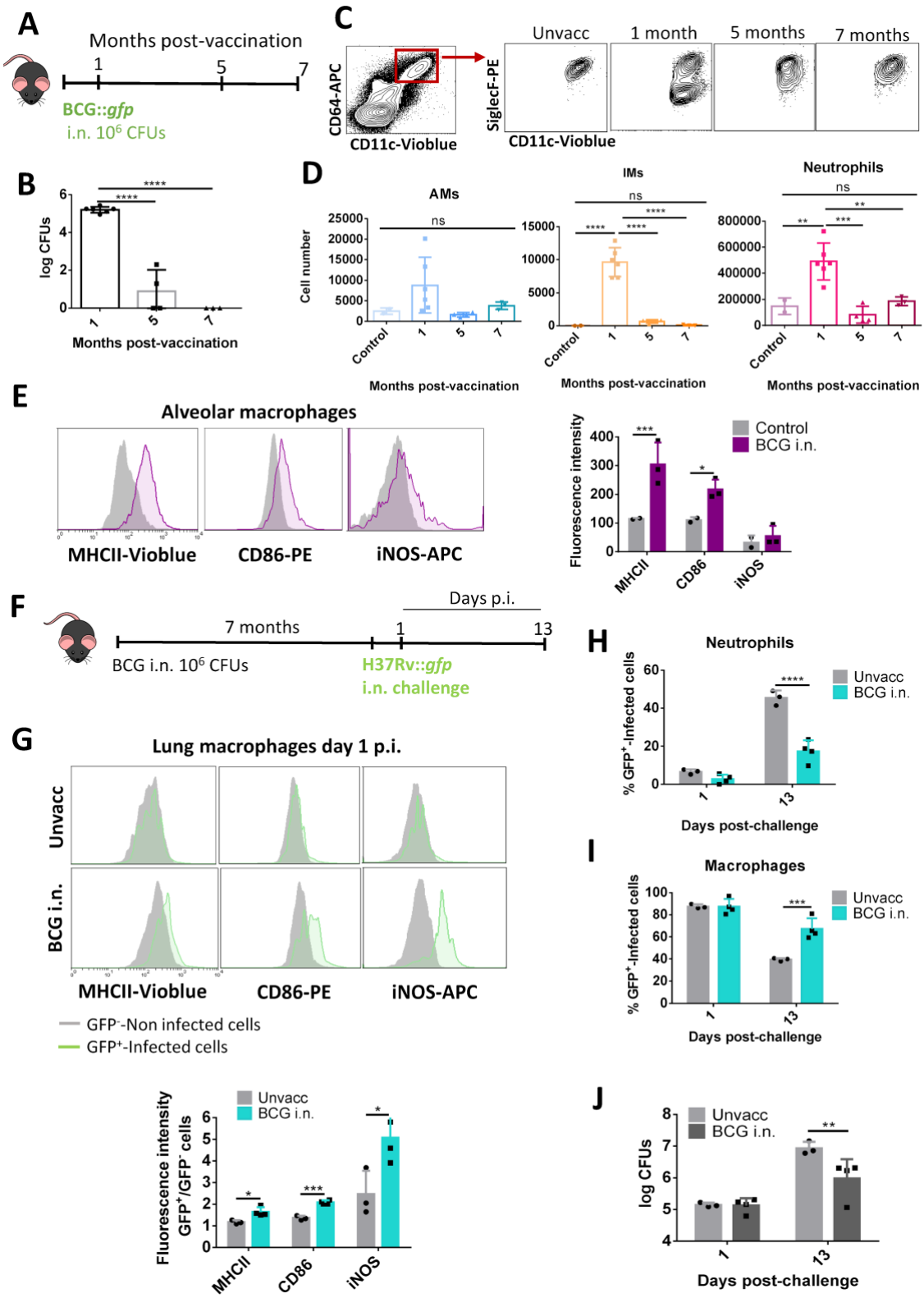

881

Fig. 5. BCG-activated macrophages retain protective capacity after vaccine clearance. A. Schema of GFP-tagged BCG vaccination by i.n. route. **B.** BCG CFUs in lungs. **C.** Representative dot-plots analyzing lung populations by expression of CD11c, CD64, and SiglecF markers. **D.** Numbers of total lung alveolar macrophages (AMs), interstitial macrophages (IMs) and neutrophils. Controls correspond to unvaccinated mice. **E.** Representative histograms and fluorescence intensity of MHCII, CD86 and iNOS expression in total macrophages at month 7 post-vaccination, in unvaccinated (grey) and i.n. BCG-vaccinated (purple) mouse groups. **F.** Schema of i.n. vaccination with non-fluorescent BCG in mice, and subsequent i.n. challenge with GFP-expressing H37Rv (H37Rv::*gfp*). **G.** Representative histograms MHCII, CD86 and iNOS expression in non-infected (grey) and *Mtb*-infected (GFP+, green) lung macrophages from unvaccinated and i.n. BCG-vaccinated mice measured one day post-infection (p.i.) with GFP-tagged H37Rv. Graph shows ratios of fluorescence intensities between GFP+ and GFP- cells for each marker and vaccination status. **H.** Frequencies of *Mtb*-infected neutrophils in unvaccinated and BCG-vaccinated mouse groups. **I.** Frequencies of *Mtb*-infected macrophages in unvaccinated and BCG-vaccinated groups. **J.** *Mtb* bacterial loads in lungs in unvaccinated and BCG-vaccinated mice. Data are representative of two experiments (n = 2-6 mice/group). Graphs are presented as mean ± SD. ns, non-significant *$p < 0.05$; **$p < 0.01$; ***$p < 0.001$; ****$p < 0.0001$ by one-way ANOVA with Bonferroni post-test (**B, D**), multiple unpaired t-student test (**e, g**), and two-way ANOVA with Bonferroni post-test (**H-J**).

SUPPLEMENTARY MATERIALS

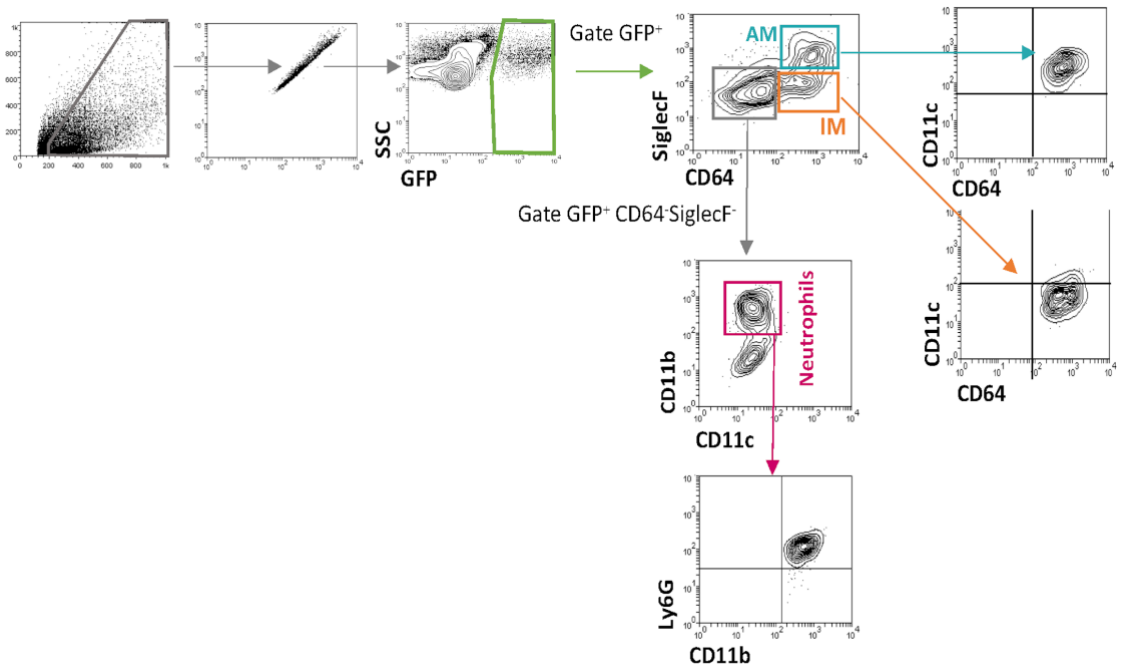

Fig. S1. Gating strategy to define AMs, IMs and neutrophils.

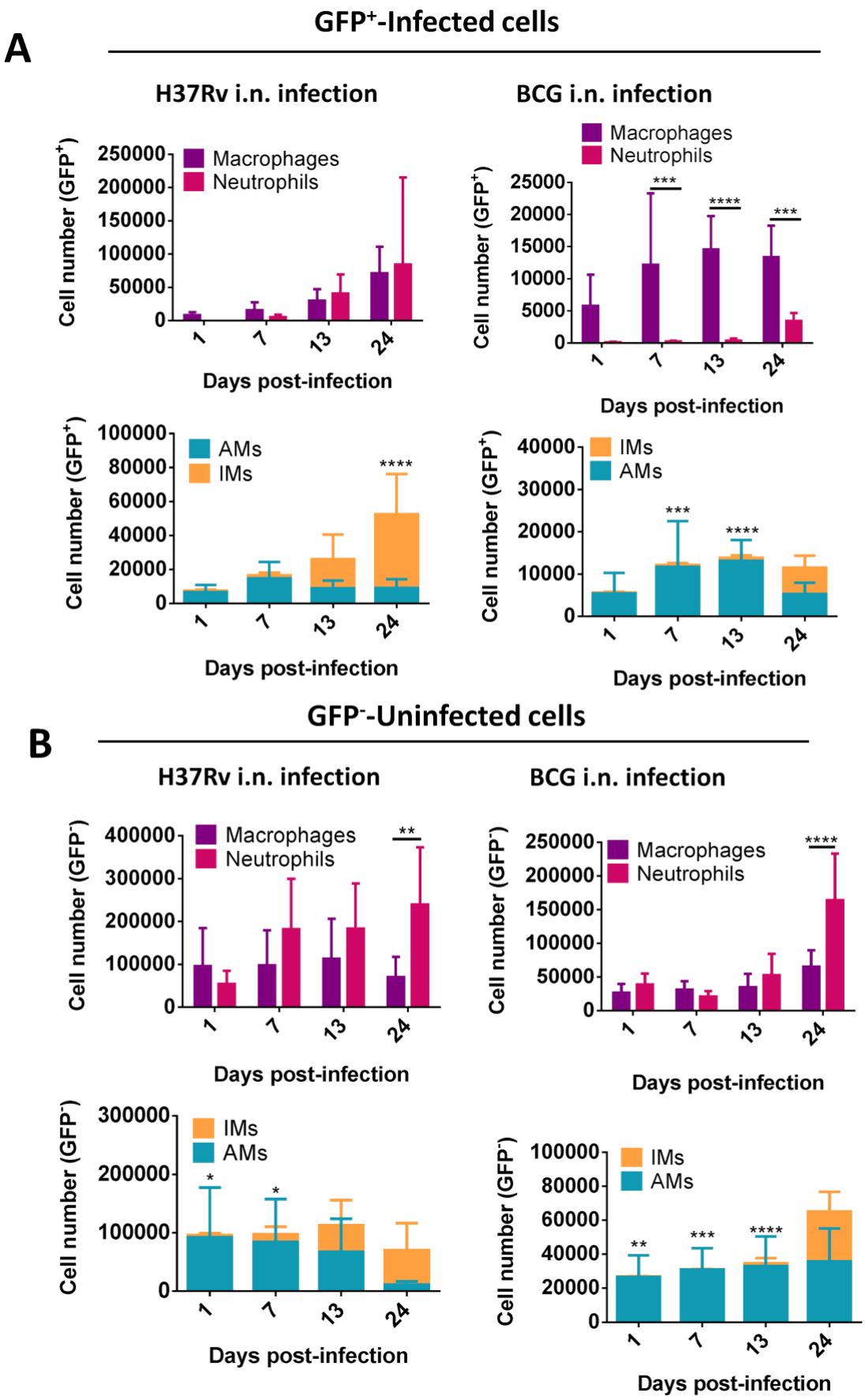
A
GFP+-Infected cells
H37Rv i.n. infection
BCG i.n. infection
Macrophages
Neutrophils
Cell number (GFP+)
Days post-infection
AMs
IMs
B
GFP--Uninfected cells
Cell number (GFP-)

908

Fig. S2. H37Rv or BCG infected and uninfected lung cells. A. Number of *Mtb* or BCG-infected macrophages, neutrophils, AMs and IMs in lungs from mice infected i.n. with GFP-tagged H37Rv or BCG**. B.** Number of uninfected macrophages, neutrophils, AMs and IMs in lungs from mice infected i.n. with GFP-tagged H37Rv or BCG. Pooled data from two independent experiments (n=6 mice/group). Graphs are presented as mean ± SD. *p < 0.05; **p < 0.01; ***p < 0.001; ****p < 0.0001 by two-way ANOVA with Bonferroni post-test.

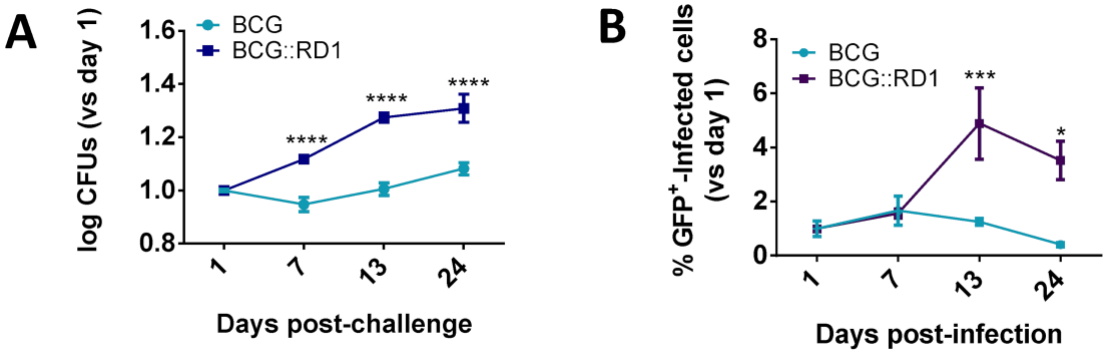

Fig. S3. RD1 complemented BCG stain restored virulence compared to BCG. A. BCG and BCG::RD1 bacterial loads in lungs normalized to day 1 post-infection. **B.** Percentage of total BCG and BCG::RD1- infected lung cells normalized to day 1 post-infection. Pooled data from two independent experiments (n=6 mice/group). Graphs are presented as mean ± SD. *p < 0.05; ***p < 0.001; ****p < 0.0001 by two-way ANOVA with Bonferroni post-test.

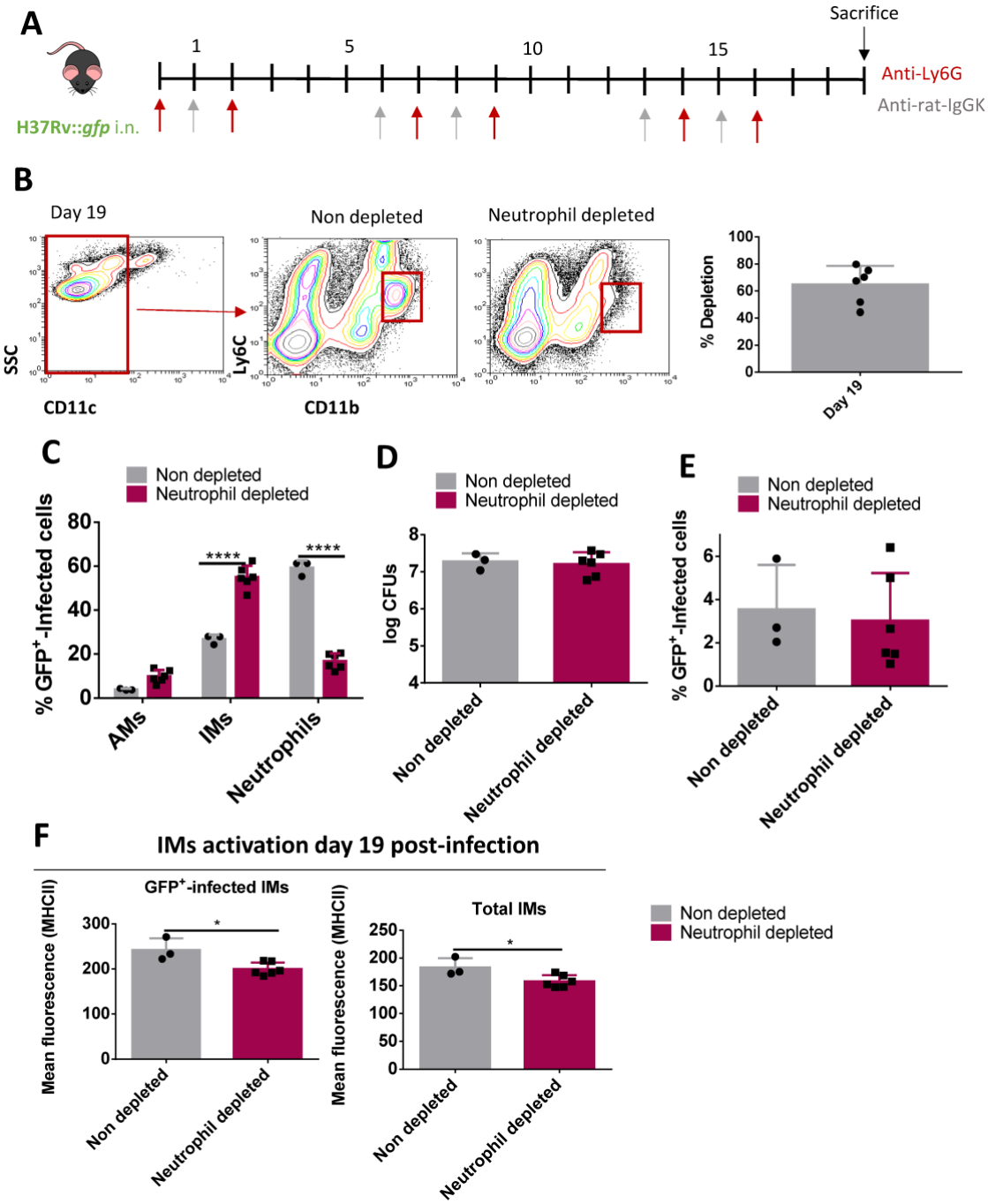

926

927 **Fig. S4. Depletion of neutrophils during *Mtb* infection**. **A.** Schema of *in vivo* neutrophil
928 depletion protocol by i.p injection of alternated anti-Ly6G and anti-rat-IgGK antibodies
929 following GFP-tagged H37Rv i.n. infection. **B.** Representative dot-plots of neutrophils in
930 lungs and proportion of neutrophils depleted in lungs from the depleted group at day 19
931 post-infection.**c,** H37Rv bacterial loads in lungs at day 19 post-infection. **D.** Percentage
932 of H37Rv-infected lung cells at day 19 post-infection. **E.** Frequencies of *Mtb*-infected

AMs, IMs and neutrophils in lungs from H37Rv infected mice. **F.** Fluorescence intensity of MHCII expression gated on H37Rv-infected macrophages at day 19 post-infection. Data are representative of one experiment (n=6 mice/group). Graphs are presented as mean ± SD. *$p < 0.05$; ****$p < 0.0001$ by unpaired t-test (c,d,f) and two-way ANOVA with Bonferroni post-test (e).

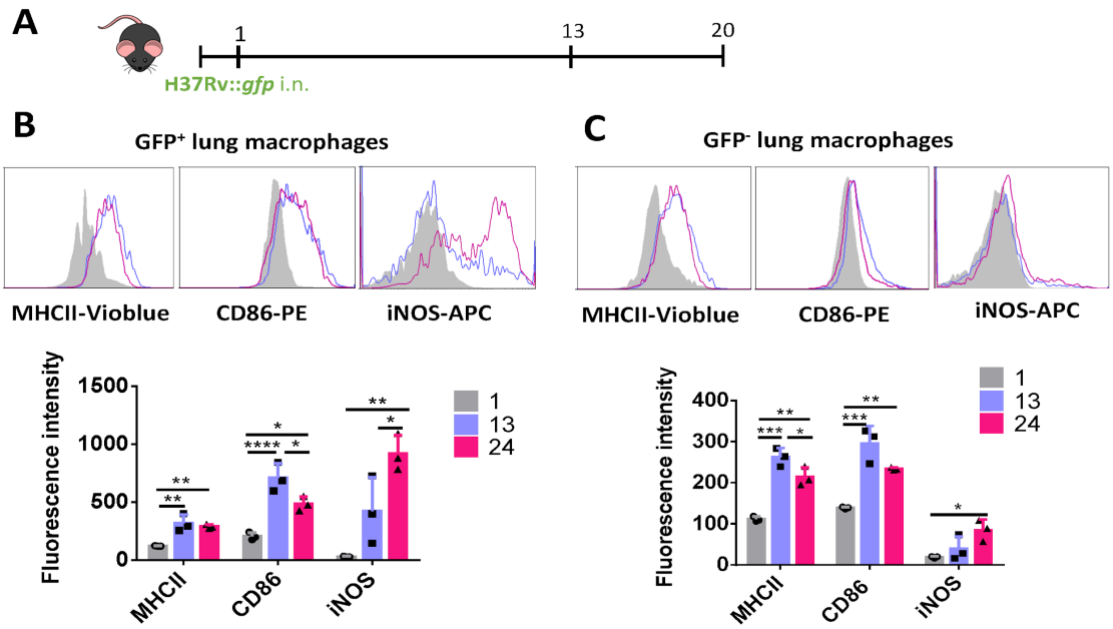

939

940 **Fig. S5. *Mtb* infection induces activation of infected and non-infected macrophages.**

941 **A.** Schema of GFP-tagged *Mtb* intranasal infection measured in days post-infection (p.i.).

942 **B.** Representative histograms and fluorescence intensity of MHCII, CD86 and iNOS

943 expression gated on BCG-infected macrophages (GFP+) at days 1 (grey), 7 (yellow), 13

944 (blue) and 20 (pink) post-infection. **C.** MHCII, CD86 and iNOS expression by non-

945 infected macrophages (GFP-). Data are representative of two independent experiments (n

946 = 3 mice/group). Graphs are presented as mean ± SEM. *p < 0.05; **p < 0.01; ***p <

947 0.001; ****p < 0.0001 by one-way ANOVA with Bonferroni post-test.

948

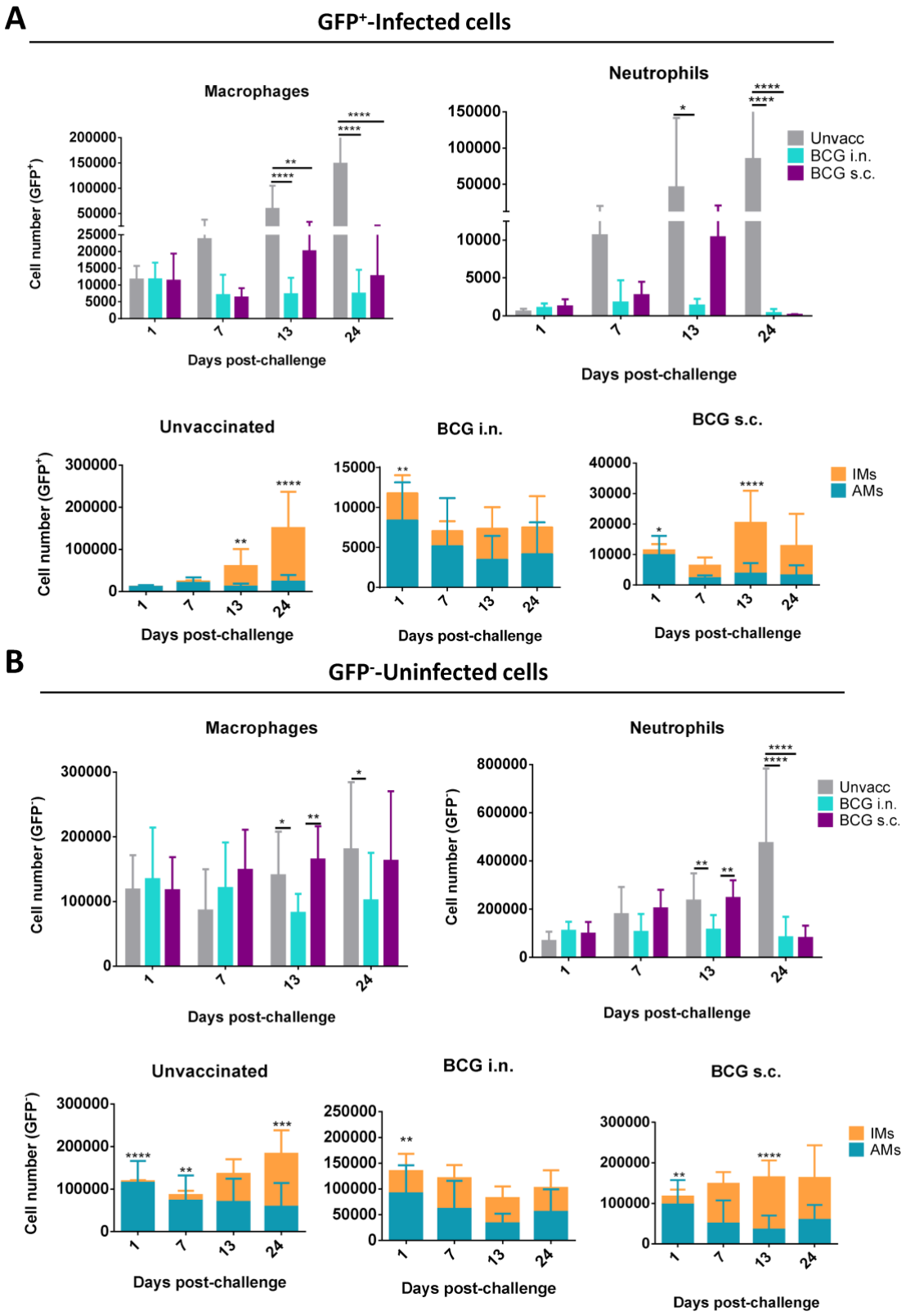

949

950 **Fig. S6. H37Rv infected and uninfected lung cells after i.n. or s.c. vaccination. A.**
951 Number of *Mtb*-infected macrophages, neutrophils, AMs and IMs in lungs from
952 unvaccinated, s.c. BCG-vaccinated and i.n. BCG-vaccinated mice. **B.** Number of

uninfected macrophages, neutrophils, AMs and IMs in lungs from unvaccinated, s.c. BCG-vaccinated and i.n. BCG-vaccinated mice after *Mtb* challenge. Pooled data from two independent experiments (n=6 mice/group). Graphs are presented as mean ± SD. *p < 0.05; **p < 0.01; ***p < 0.001; ****p < 0.0001 by two-way ANOVA with Bonferroni post-test.

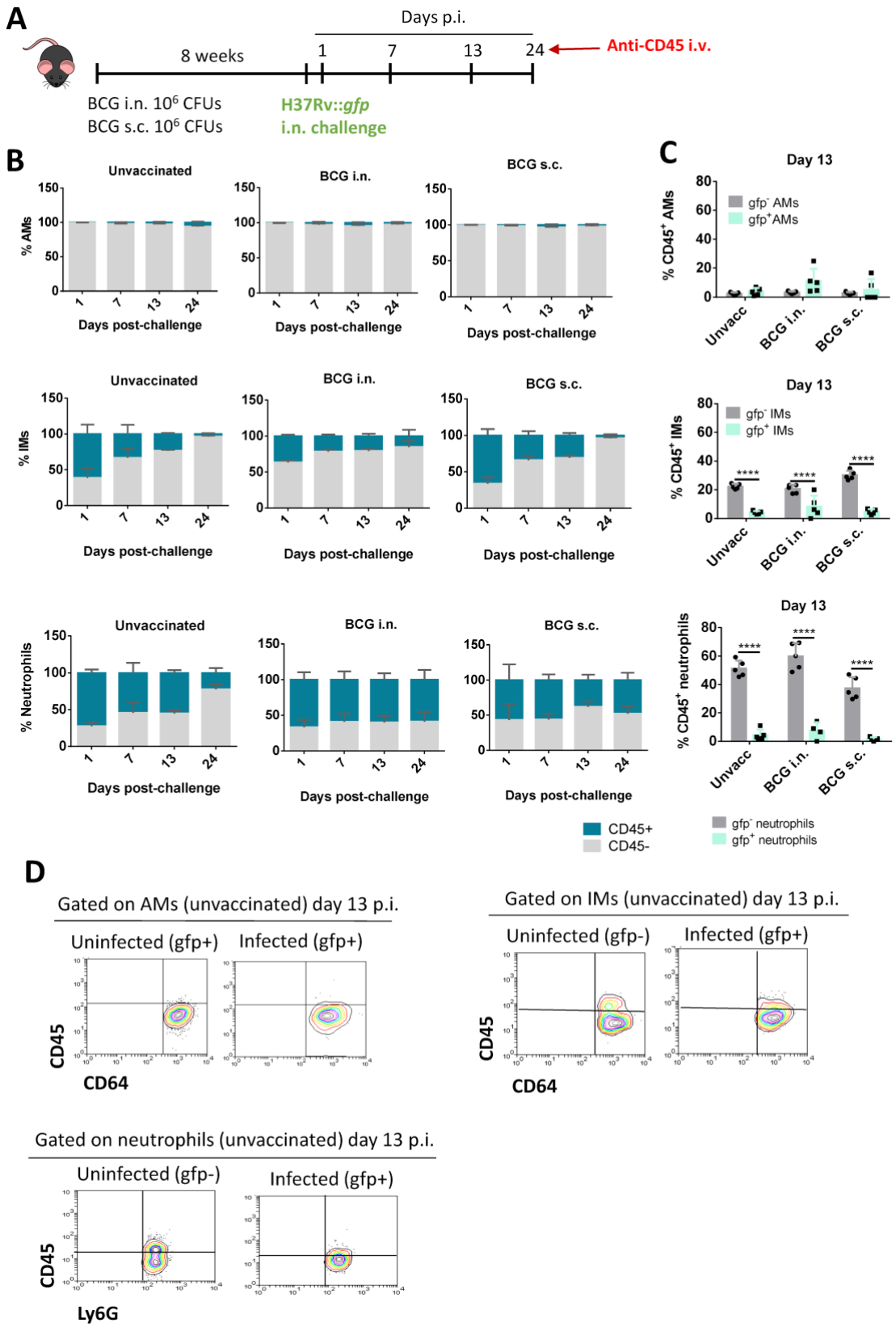

Fig. S7. Compartmentalization of AMs, IMs and neutrophils in lungs after Mtb challenge. A. Schema of i.n. and s.c. vaccination of mice with non-fluorescent BCG and

subsequent i.n. challenge with GFP-expressing H37Rv. Anti-CD45 antibody was administered i.v. prior to sacrifice. **B.** Frequencies of total CD45+ and CD45- lung AMs, IMs and neutrophils in unvaccinated, s.c. BCG-vaccinated and i.n. BCG-vaccinated mice. **C.** Frequencies of GFP+-infected and GFP--uninfected CD45+ AMs, IMs and neutrophils in unvaccinated, s.c. BCG-vaccinated and i.n. BCG-vaccinated mice at day 13 post-challenge. **D.** Representative dot plots of CD45 expression in GFP+-infected and GFP--uninfected AMs, IMs and neutrophils in unvaccinated, s.c. BCG-vaccinated and i.n. BCG-vaccinated mice at day 13 post-challenge. Data are representative of one experiment (n=6 mice/group). Graphs are presented as mean ± SD. ****$p < 0.0001$ by two-way ANOVA with Bonferroni post-test.

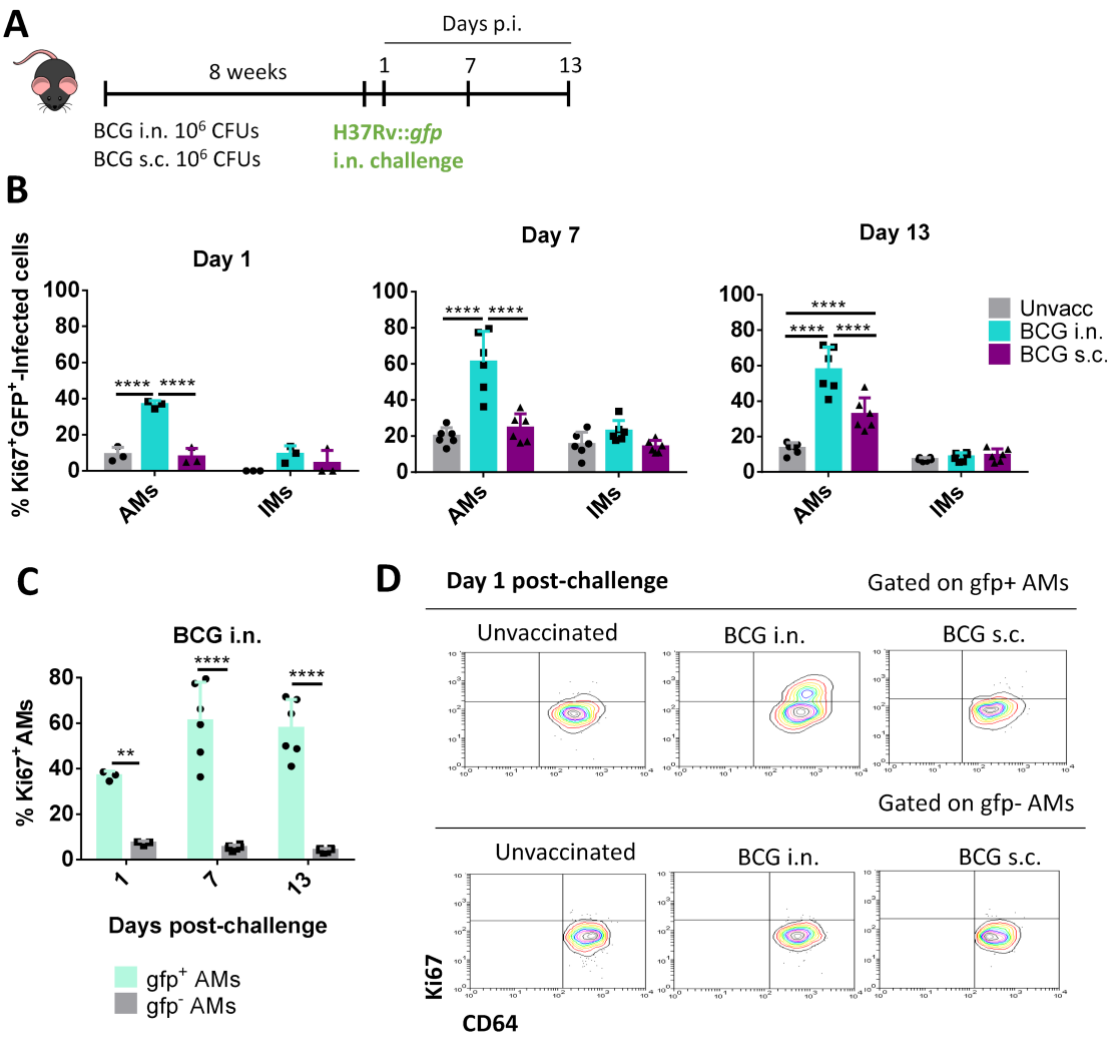

974

975 **Fig. S8. Pulmonary BCG vaccination induces Ki67 expression in *Mtb*-infected AMs**
976 **upon challenge. A.** Schema of i.n. and s.c. vaccination of mice with non-fluorescent BCG
977 and subsequent i.n. challenge with GFP-expressing H37Rv. **B.** Frequencies of *Mtb*-
978 infected AMs and IMs expressing Ki67 in unvaccinated, s.c. BCG-vaccinated and i.n.
979 BCG-vaccinated mice. **C.** Frequencies of in GFP^+-infected and GFP^--uninfected AMs
980 expressing Ki67 in i.n. BCG vaccinated mice at day 13 post-challenge. **D.** Representative
981 dot plots of Ki67 expression in GFP^+-infected and GFP^--uninfected AMs in unvaccinated,
982 s.c. BCG-vaccinated and i.n. BCG-vaccinated mice at day 1 post-challenge. Data are
983 representative of one experiment (n=6 mice/group). Graphs are presented as mean ± SD.
984 ****$p < 0.0001$ by two-way ANOVA with Bonferroni post-test.

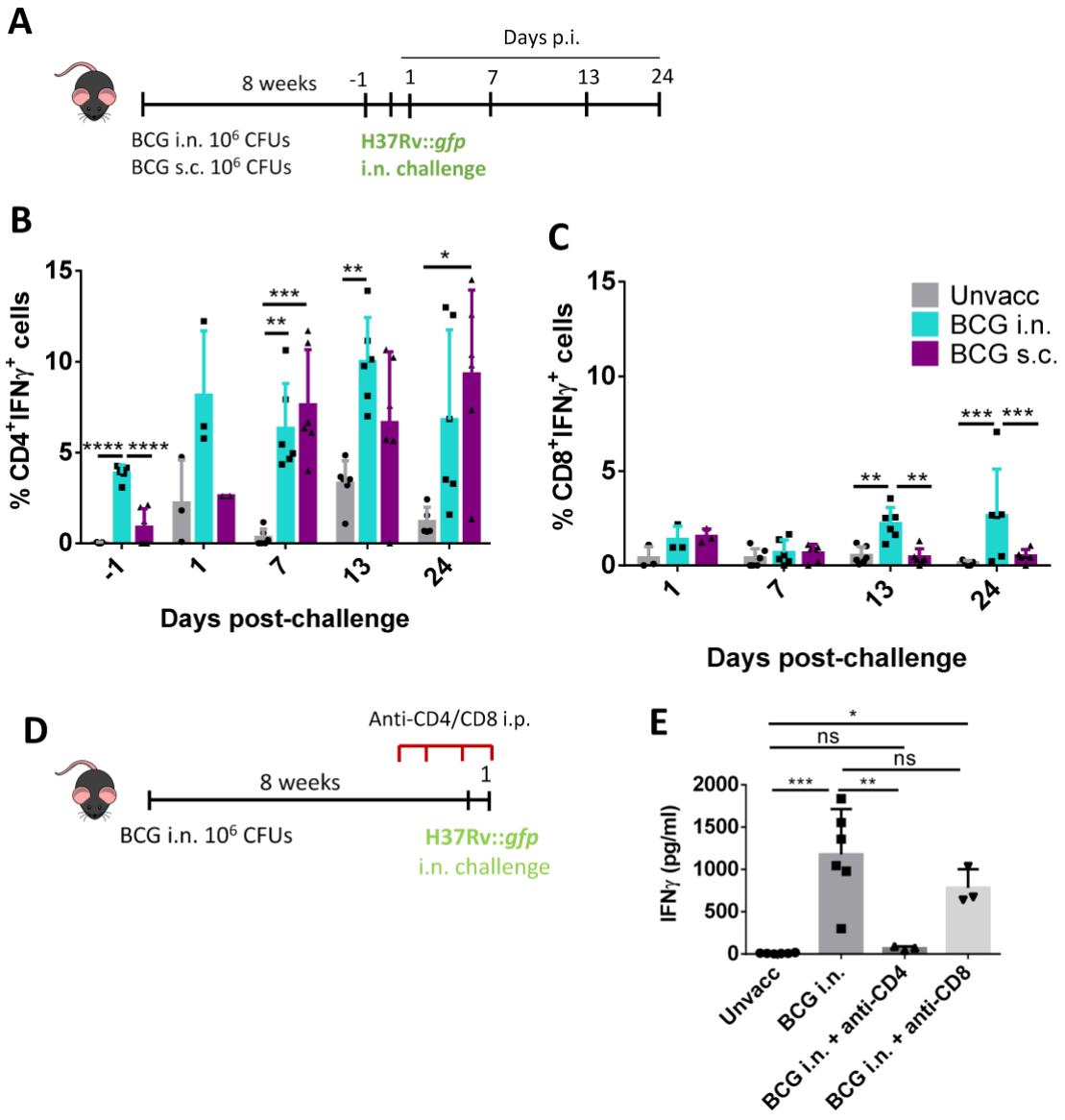

985

986 **Fig. S9. CD4⁺ cells are the main source of IFNγ production in lungs during *Mtb***
987 **infection. A.** Schema of i.n. and s.c. vaccination of mice with non-fluorescent BCG and
988 subsequent i.n. challenge with GFP-expressing H37Rv. **B.** Frequencies of IFNγ⁺ CD4 T
989 cells in lungs of unvaccinated, s.c. BCG-vaccinated and i.n. BCG-vaccinated mice after
990 PPD stimulation of lung cells. **C.** Frequencies of IFNγ⁺ CD8 T cells in lungs of
991 unvaccinated, s.c. BCG-vaccinated and i.n. BCG-vaccinated mice after PPD stimulation
992 of lung cells. **D.** Schema of i.n. vaccination of mice with non-fluorescent BCG and
993 subsequent i.n. challenge with GFP-expressing H37Rv, with CD4+ T-cell depletion
994 treatment by i.p. administration of anti-CD4 or anti-CD8 neutralizing antibodies, starting

7 days prior to i.n. H37Rv challenge. **E.** Total IFN γ production in lung cells incubated *ex vivo* from unvaccinated and i.n. BCG-vaccinated mice at day 1 post-challenge. Data are representative of one experiment (n=6 mice/group). Graphs are presented as mean ± SD. *$p < 0.05$; **$p < 0.01$; ***$p < 0.001$ by two-way ANOVA with Bonferroni post-test (**B, C**) and one-way ANOVA with Bonferroni post-test (**E**).

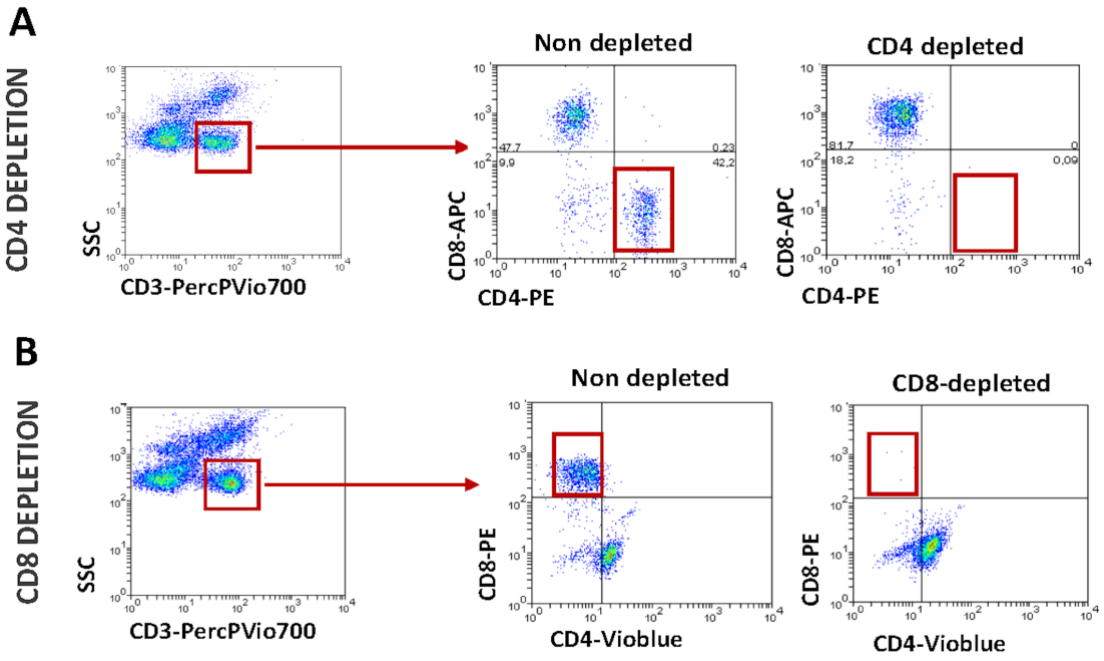

Fig. S10. Efficacy of CD4$^+$ and CD8$^+$ cells depletion by antibody treatment.

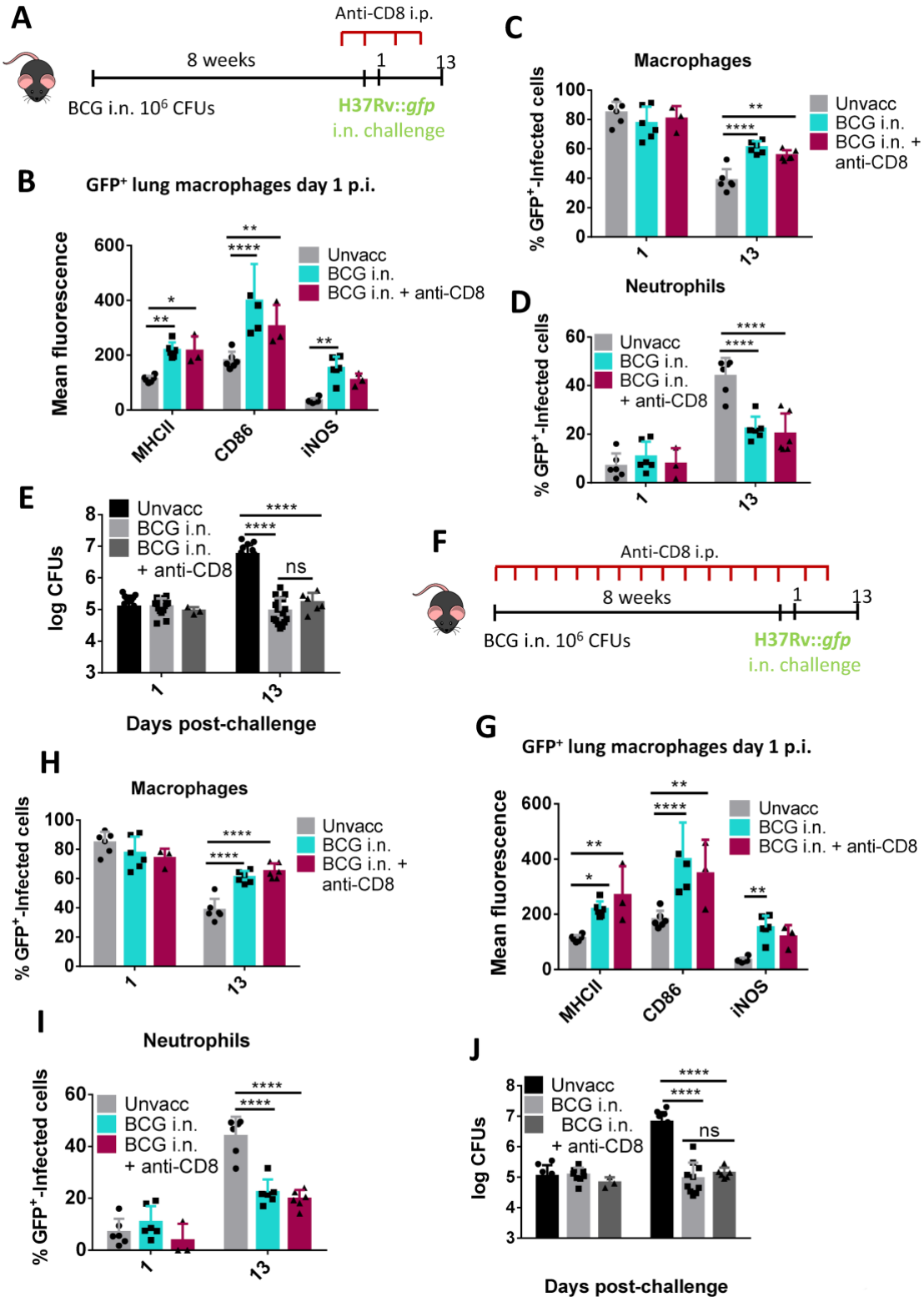

1005

1006 **Fig. S11. BCG-activated macrophages protection in the absence of CD8⁺ cells. A.**

1007 Schema of i.n. vaccination with non-fluorescent BCG in mice, and subsequent i.n.

1008 challenge with GFP-expressing H37Rv, with CD8+ T-cell depletion treatment by i.p.

administration of anti-CD8 neutralizing antibodies, starting 7 days prior to i.n. H37Rv challenge. **B.** Fluorescence intensity of MHCII, CD86 and iNOS expression gated on H37Rv-infected macrophages at day 1 post-challenge, in unvaccinated (grey), i.n. BCG-vaccinated (blue) and i.n. BCG-vaccinated CD8+-depleted (red) groups. **C.** Frequencies of *Mtb*-infected macrophages in unvaccinated (grey), i.n. BCG-vaccinated (blue) and i.n. BCG-vaccinated CD8+cells-depleted (red) mice. **D.** Frequencies of *Mtb*-infected neutrophils in unvaccinated (grey), i.n BCG-vaccinated (blue) and i.n. BCG-vaccinated CD8+cells-depleted (red) mice. **E.** *Mtb* bacterial loads in lungs in unvaccinated, i.n. BCG -vaccinated and i.n. BCG-vaccinated CD8+cells-depleted mice. **F.** Scheme of i.n. vaccination of mice with non-fluorescent BCG, and subsequent i.n. challenge with GFP-expressing H37Rv, with i.p. CD8+ cell-depletion treatment, starting 7 days prior to i.n. BCG vaccination. **G.** Fluorescence intensity of MHCII, CD86 and iNOS expression gated on H37Rv-infected macrophages at day 1 post-challenge, in unvaccinated (grey), i.n. BCG-vaccinated (blue) and i.n. BCG-vaccinated CD8+cells-depleted (red) mouse groups. **H.** Frequencies of *Mtb*-infected macrophages in unvaccinated (grey), i.n. BCG-vaccinated (blue) and i.n. BCG-vaccinated, CD8+cells-depleted (red) mice. **I.** Frequencies of *Mtb*-infected neutrophils in unvaccinated (grey), i.n. BCG-vaccinated (blue) and i.n. BCG-vaccinated, CD4+cells-depleted (red) mice. **J.** *Mtb* bacterial loads in lungs of unvaccinated, i.n. BCG-vaccinated and i.n. BCG-vaccinated CD8+cells-depleted groups. Data are representative of one experiment (n = 6 mice/group). Graphs are presented as mean ± SD. ns, non-significant *$p < 0.05$; **$p < 0.01$; ****$p < 0.0001$ by one-way ANOVA with Bonferroni post-test **(B, G**), and two-way ANOVA with Bonferroni post-test (**C-E, H-J**).

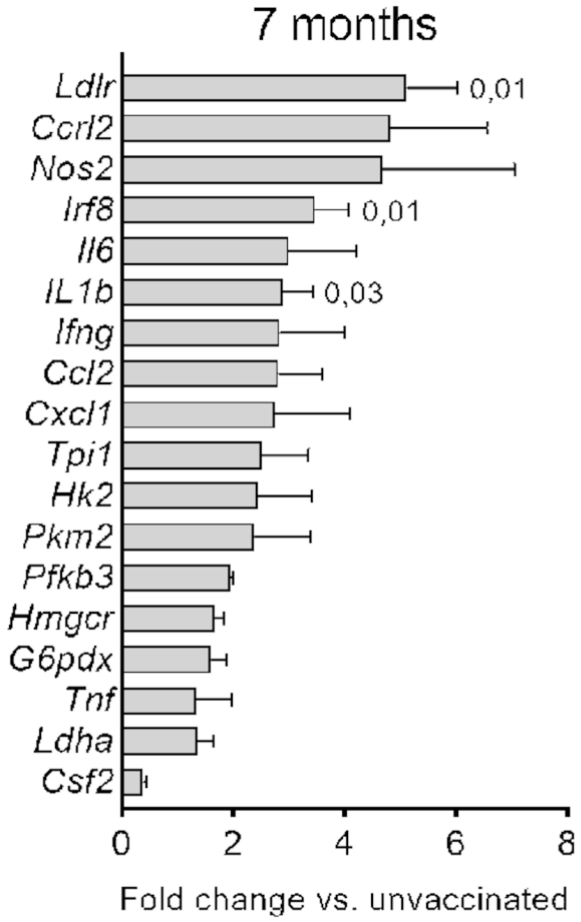

1033

1034

1035 **Fig. S12. AMs gene expression analysis after 7 months post-vaccination.** Relative

1036 gene expression of sorted AMs from BCG i.n. vaccinated mice 7 months post-vaccination.

1037

Table S1. Antibodies used for flow cytometry cell characterization

ANTIBODY	SOURCE	IDENTIFIER
Anti-mouse CD11c PE	Miltenyi Biotec	Cat#130-102-545; RRID: AB_2660154
Anti-mouse CD11c Vioblue	Miltenyi Biotec	Cat#130-102-413; RRID: AB_2660158
Anti-mouse CD11b PerCP-Vio700	Miltenyi Biotec	Cat#130-113-809; RRID: AB_2751174
Anti-mouse Siglec-F PE	Miltenyi Biotec	Cat#130-102-274; RRID: AB_2653451
Anti-mouse Siglec-F APC	Miltenyi Biotec	Cat#130-102-241; RRID: AB_2653452
Anti-mouse CD64 APC	Miltenyi Biotec	Cat#130-103-809; RRID: AB_2658943
Anti-mouse Ly6G VioBlue	Miltenyi Biotec	Cat#130-119-986; RRID: AB_2751964
Anti-mouse MHCII VioBlue	Miltenyi Biotec	Cat#130-102-145; RRID: AB_2660060
Anti-mouse CD86 PE	BD Biosciences	Cat#553692; RRID: AB_394994
Anti-mouse iNOS APC	Miltenyi Biotec	Cat#130-116-423; RRID: AB_2727527
Anti-mouse CD45 FITC	Miltenyi Biotec	Cat#130-110-796; RRID: AB_2658216
Anti-mouse CD45 PerCP-Vio 700	Miltenyi Biotec	Cat# 130-110-663, RRID:AB_2658233
Anti-mouse CD3 PerCP-Vio 700	Miltenyi Biotec	Cat#130-120-826; RRID: AB_2752207
Anti-mouse CD4 PE	BD Biosciences	Cat#553653; RRID:AB_394973
Anti-mouse CD8a APC	Miltenyi Biotec	Cat#130-102-808; RRID:AB_2659886
Anti-IFNγ APC	Miltenyi Biotec	Cat# 130-123-283, RRID:AB_2819467
Anti-Ki67 PerCPVio700	Miltenyi Biotec	Cat# 130-120-560, RRID:AB_2784394
FcR blocking	Miltenyi Biotec	Cat#: 130-092-575

1042 **Table S2. Primer sequences used for gene expression analysis**

GENE	FORWARD 5'-3'	REVERSE 5'-3'
Ifnγ	ATGAACGCTACACACTGCATC	CCATCCTTTTGCCAGTTCCTC
Cxcl1	TGGCTGGGATTCACCTCA A	GAGTGTGGCTATGACTTC GGTT
Tnfα	ACGGCATGGATCTCAAAGAC	GTGGGTGAGGAGCACGTAGT
Il6	CCGGAGAGGAGACTTCA CAG	TCCACGATTTCCCAGAGAAC
GK	TGAGCCGGATGCAGAAGGA	GCAACATCTTTACACTGGCCT
IL1β	GCAACTGTTCCTGAACTCAACT	ATCTTTTGGGGTCCGTCAACT
Nos2	CGTTTCGGGATCTGAATGTGA	GGGCAGCCTGTGAGACCTT
Irf8	AGACCATGTTCCGTATCCCCT	CACAGCGTAACCTCGTCTTCC
Ccrl2	CCCCGGACGATGAATATGATG	CACCAAGATAAACACCGCCAG
Ccl2	TAAAAACCTGGATCGGAA CCAA	GCATTAGCTTCAGATTTACGGGT
Csf2	GGCCTTGGAAGCATGTAGAGG	GGAGAACTCGTTAGAGACGACT T
Eno1	TGCGTCCACTGGCATCTAC	CAGAGCAGGCGCAATAGTTTTA
Ldlr	TCAGACGAACAAGGCTG TCC	CCATCTAGGCAATCTCGGTCTC
Hmgcr	TGTTCACCGGCAACAACAAGA	CCGCGTTATCGTCAGGATGA
G6pd2	AGGTGACCCTAAGCCGGAC	AGGTTTCTTTGGGTAGAA GACA
G6pdx	CACAGTGGACGACATCCGAAA	GCAGGGCATTCATGTGGCT
Ldha	TGCCTACGAGGTGATCAA GCT	GCACCCGCCTAAGGTTCTTC
Hk2	CCGCCGTGGTGGACAAGA TA	AGCAGTGATGAGAGCCGCTC
B2m	CTGGTCTTTCTGGTGCTTGTC	GTATGTTCGGCTTCCCATTC
Pfkpb1	TCACACCTGTGGCTTATG GCTGC	GGGGTTCCTCGGGTTCACGG
Pfkpb3	GGCATATGGGTGCCGGGTGG	GGTGGGCTCGGGACTGGCTA
Pkm2	CGCCTGGACATTGACTCTGA	GAAATTCAGCCGAGCCACATT
Tpi1	CAAACCAAGGTCATCGCAGA	GCCCACACAGGTTCATAGGC

1043

1044